Lightweight gearbox housing with enhanced vibro-acoustic behavior through the use of locally resonant metamaterials

Daniel Rocha Amaral, Mohamed Najib Ichchou, Przemyslaw Kolakowski, Pascal Fossat, Michelle Salvia

Lightweight gearbox housing with enhanced vibro-acoustic behavior through the use of locally resonant metamaterials

D.R. Amaral[a,*], M.N. Ichchou[a], P. Kołakowski[b], P. Fossat[a], M. Salvia[a]

[a] *LTDS, Laboratoire de Tribologie et Dynamique des Systems, Ecole Centrale de Lyon, France*
[b] *Adaptronica sp. z o.o., Łomianki, Poland*

Abstract

Mass reduction of automotive components enhances vehicles' performance and extends their driving range. However, lightweight construction typically leads to noise and vibration issues. Hence, the development of lightweight components must go in tandem with advancements in the field of noise and vibration. This work focuses on the lightweighting of the gearbox housings (GBHs) and on the introduction of vibroacoustic metamaterials to improve their Noise, Vibration, and Harshness (NVH) characteristics. Topology optimization methods were used to reduce the mass of a GBH. Its noise emission was evaluated numerically, before and after the mass reduction. Locally resonant metamaterial (LRM) solutions were applied in the GBH and then tested in numerical simulations. This analysis showed the LRM solutions reduce the emission of noise in the predicted band gaps (BGs), while also providing significant attenuation across the entire frequency spectrum under consideration. The experimental results confirmed the effectiveness of the LRM attenuation concept and the trends observed in the numerical results. Vibration was also attenuated in parts of the GBH where the LRM was not applied. Attenuation of in-plane housing vibration was also observed. The proposed LRM solutions are lightweight, passive and low-cost solutions that can implemented in housings to enhance their NVH characteristics.

Keywords:
gearbox housing, lightweight design, NVH control, locally resonant metamaterials

*Corresponding author
Email address: daniel.amaral@ec-lyon.fr (D.R. Amaral)

1. Introduction

Solutions to diminish the human impact on climate change are urgently needed. Our impact on the environment is significantly influenced by transportation and mobility. Reducing the mass of vehicles constitutes a clear benefit for decreasing the environmental impacts of transport and mobility, providing more energy-efficient solutions.

Reducing the mass of vehicles' components is the way to lower vehicles' overall weight. Automotive component weight reduction can significantly enhance a vehicle's performance by extending its driving range, since lighter cars use less energy to accelerate and maintain speed. Reduced component weight can also enhance the vehicle's handling and agility, making it more responsive and simple to maneuver. In the case of ICE vehicles, the mass reduction also leads to better fuel economy and a decrease in emissions of greenhouse gases and other noxious gases and particles.

In order to produce lightweight automotive parts, they should be manufactured with lightweight materials and designed using less material while providing the necessary strength and functionality. However, laws of physics reveal that, as a general rule, lightweight components radiate more noise than their original counterparts due to their higher stiffness-to-mass ratio.

Due to noise level regulations and to satisfy consumer expectations, automakers strive to provide silent automobiles for the market. Hence, these two conflicting design objectives need to be addressed with novel solutions, such as the application of vibroacoustic metamaterials. The objective of this study is to demonstrate that the lightweight design of GBHs can be a viable option by addressing the NVH issues associated with this design. So far, gearboxes have relied on traditional methods to comply with NVH regulations. However, by leveraging recent developments in the field of metamaterials, innovative solutions can be developed.

1.1. Gearbox and its Housing Design

A gearbox is a mechanical system consisting of an arrangement of gears within a housing. Its primary function is to transmit power from a driving device to a load by altering the torque and speed of the rotational output. Gearboxes come in a variety of sizes and shapes, and their internal design can vary depending on the specific application. Typically, the gears are mounted on shafts, which are supported by bearings that enable them to rotate. These bearings are then coupled to the gearbox housing (GBH), which provides a protective enclosure for the assembly. Overall, the gearbox is a critical component in many mechanical systems, as it allows for efficient power transmission and motion control. By altering torque and speed, the gearbox can match the output of a driving device to the requirements of a load, resulting in improved performance and energy efficiency.

Gearboxes are used in wind turbines, machine tools, industrial equipment, conveyors, ships, automobiles, and aerospace applications. According to their

application, multiple requirements may arise. In automotive applications, gearboxes are used to amplify the output torque by reducing the output rotational speed, according to the set gear ratio. A gearbox with several gear ratios allows the efficient use of the power delivered from the motor.

GBHs must follow specific requirements, namely, they must support for the primary gearbox components, selector mechanisms and actuators. The GBH must ensure the correct gear meshing, respecting the assembly tolerances of the rotating components, and cope with system loading generated by the transmitted torque. Additionally, there are other requirements related with the protection of the gearbox inner components, enclosure of the lubricant, and heat dissipation capabilities.

In addition to the aforementioned requirements, an essential characteristic of a well-designed GBH is its ability to provide good NVH properties. NVH refers to the unwanted noise, vibration, and harshness that can result from the operation of the system. Good NVH characteristics not only contribute to the comfort of individuals, inside and outside the vehicle, but also improve the reliability and longevity of the gearbox system by reducing wear and tear on the components.

Typically, gearbox housings are made of cast metal alloys, such as iron, aluminum, or magnesium. In the industry, these housings are traditionally manufactured by casting, and the production volume determines the type of casting used. For low volumes, sand casting is used, while high-volume production relies on die casting.

The reduction of mass while preserving the design function is the core of the lightweight design approach. For this purpose, topology optimization methods can contribute, enabling multi-objective optimization of the housing geometry. Topology optimization is a mathematical method that optimizes the material distribution within a specified design space while respecting defined constraints. When aiming to maximize the stiffness of a structure, the compliance of the structure should be minimized. In addition to the objective function, constraints can be introduced to ensure that the design meets specific criteria. For example, constraints can limit the maximum von Mises stress below the material strength or the maximum displacement in the bearings below a predetermined value. In the literature, some works can be found on the topic of structural optimization of GBHs [1, 2, 3]. However, they do not investigate the NVH issues resulting from the mass reduction of the gearbox housing.

Given the structural and functional similarities between gearbox housings and electric vehicle (EV) motor housings, it is worth noting that the findings presented in this work can be applied to EV motor housings as well.

1.2. Conventional Vibroacoustic Control Methods

The NVH (Noise, Vibration, and Harshness) characteristics of a component are firstly determined by its design, as well as its structural and dynamic properties. Therefore, design modifications to the component will change its NVH characteristics. Stiffeners are largely used to increase the components' global

stiffness. Two vibroacoustic consequences occur with the introduction of stiffeners in a structure: a decrease in vibration levels and an increase in radiation efficiency [4]. Depending on which effect dominates, sound radiation can increase or decrease. The radiation efficiency increases due to near-field vibration components next to the stiffeners, which radiate sound more efficiently [5].

Generally, adding mass to a component is a way of reducing vibration and noise emissions. However, the mass increment far from the excitation point is ineffective in decreasing vibration levels or sound radiation [5]. Moreover, it goes against the objective of the lightweight design concept. Another common practice to reduce noise radiation from components is the application of acoustic treatment material layers with high sound absorption coefficients. These materials are designed to vibrate and dissipate sound energy as heat, thereby reducing the amount of noise that is radiated from the component. In order to maximize the absorption of sound waves, it is essential to apply the absorptive material with a thickness of one-quarter wavelength on the surface of the vibrating structure. Sound waves induce variations in pressure and particle velocity. At one-quarter wavelength distance from the radiating surface, there is low pressure and high fluid particle velocity, making it the most effective region for sound absorption. It is important to note that a thick layer of acoustic treatment material is needed to attenuate low frequencies, making this method inefficient [6]. Another method is through the introduction of reflective partitions into the transmission path, which induce a high change of acoustic impedance, a method that is commonly used in ICE vehicle exhaust expansion chambers. These two methods are also used in synergy, for example in automobile dash panel structures [6].

Finally, active control methods can be employed to enhance NVH properties. However, these methods increase substantially the complexity and cost of the system and should be considered only if other passive measures have proven ineffective [5].

1.3. Metamaterials and Vibroacoustic Metamaterials

In nature, we can find different materials and even cellular solids, such as cork, wood, coral, sponge, and honeycomb [7]. Conversely, metamaterials are man-made structures that are designed to have unique physical properties that cannot be found in conventional materials [8]. The prefix "meta" comes from the Greek word, $\mu\epsilon\tau\acute{\alpha}$, which means "beyond". Metamaterial's unique properties derive from their designed microstructures. The study and development of metamaterials started in the electromagnetic domain and then was extended to the mechanical domain and, more specifically, to the field of vibroacoustics [9]. The physics of the metamaterials can be highly counter-intuitive, inducing a burst of new research [10, 11, 12].

Metamaterials are a novel class of complex engineered materials, and generally they take the form of unit cell (UC) assemblies of non-homogeneous material composition and/or topology. The topic generated enthusiasm in the scientific community since they can be designed to exhibit unconventional electromagnetic, acoustic or mechanical properties. Depending on the physics field, meta-

material characteristics are vast and diverse. The electromagnetic metamaterials' distinct characteristics are, for example, negative refraction, waveguiding characteristics or cloaking [13, 14, 15, 16, 17]. In the literature, mechanical metamaterials are categorized in subgroups, for example: Pentamode metamaterials (or meta-fluid) which are able to deform without changing their volume; Auxetic metamaterials (dilational materials), which are characterized by the increase in transverse dimension when an axial tensile load is applied to it, or in other words, materials with a negative Poisson's ratio; Metamaterials with negative stiffness; or even metamaterials with bi-stable UCs. In the bibliography, a vast range of mechanical metamaterials are lattice materials, which are open-cell cellular materials composed of a large number of architected structural elements, such as slender beams or rods [7, 8, 18, 19, 20, 21]. In order to control elastic and acoustic waves, vibroacoustic metamaterials are nowadays applied in several fields. Harmful consequences of seismic waves on man-made structures can be prevented through the use of seismic metamaterials [22, 23, 24]. Along with the study of new metamaterials, new applications for them can be sought and mastered. The recent developments in computational methods may, as well, allow synergies between topology and material composition to reach unprecedented properties for engineering applications [7].

The most outstanding functionality of metamaterials in vibroacoustics the capability of enabling strong attenuation of vibration and noise in specific frequency ranges. These frequency ranges are called band gaps (BGs) or stop bands (SBs), and in a nutshell, they are the ranges of frequencies where free wave propagation is not allowed. BG behavior was first investigated in the quantum mechanics' field, more specifically in the band-discretized movement of electrons in crystal lattices [25, 26]. The concept was transposed to electromagnetic waves [27, 28, 29], and after to elastic and acoustic wave propagation field by Sigalas and Economou [30], where they tested lattice configurations of spherical inclusions in other mediums for evaluation of BGs.

There are two types of vibroacoustic metamaterials: Phononic Crystals (PCs) and Locally Resonant Metamaterials (LRMs). PCs rely on interference-based attenuation and require periodic arrangement, while LRMs generate vibration attenuation through sub-wavelength resonant inclusions or additions.

1.3.1. Phononic Crystals

The denomination of phononic crystals (PCs) was initiated by Kushwaha et al. [31] in 1993. The concept of phononic crystals in vibroacoustics is an analogy to the other photonic crystals in electromagnetics. The prefix "phonon" derives from the Greek word "phōnē", which means sound. Photons are quantized light waves, analogously phonons can be thought of as quantized sound waves [32].

A study published in the Journal Nature in 1995 presented experimental sound attenuation results through a 2D periodic sculpture constituted by several steel cylinders [33]. The mentioned structure is a PC, once the attenuation of the propagation of acoustic waves is due to the periodicity of the arrangement near the Bragg interference frequency region. Based on this first study, two years later, Kushwaha [34] performed computations for two-dimensional periodic

arrays of rigid stainless steel cylinders in the air. Goffaux et al. [35] investigated experimentally the sound attenuation reached in the BGs for finite thickness PC samples and realized a comparison with the mass law. Additional studies were carried out in this area, studying the lattice layout effects on the sound attenuation [36, 37].

Phononic Crystals are not restricted to solid inclusions on fluid mediums. PCs can consist of solid inclusions on solid mediums. In [38], Vasseur et al. confirmed the existence of absolute acoustic BGs in two-dimensional periodic composite media, through acoustic wave transmission experiments in binary solid/solid composite media composed of arrays of duralumin cylindrical inclusions embedded in an epoxy resin matrix. By the definition found in [39], PCs are periodic structures made of different materials designed to control the propagation of mechanical waves. PCs may be one-dimensional, such as a periodic structure made of alternate homogeneous solid layers with distinct material properties [40] [41] [42]; two-dimensional, for example a lattice of vacuum cylinders in a solid background [43] or a pattern of solid cylinders in the air [33]; or three-dimensional, like the inclusion of solid spheres in another solid background material [30] [44].

Delpero et al. [45] demonstrated novel techniques for enhancing sound transmission loss across partitions using PCs. They created a three-dimensional phononic crystal with a UC designed to achieve a BG in the mid-range of the acoustic frequency spectrum. The PC was investigated experimentally and compared with conventional sandwich panels with foam cores. The performance of the phononic crystal core was remarkable in terms of amplitude reduction in the transmissibility and width of the attenuation band. However, the investigated PC core revealed a poorer static performance than the honeycomb structures and foams, traditional core options for sandwich panels. Following this work, Delpero et al. [46] introduced inertial amplification and longitudinal-torsional coupling mechanisms in the PC core to widen the BG. In 2018, Van Damme et al. [47] presented a PC consisting of a sandwich plate with inner stiffeners organized in checkerboard patterns. The inner filled spaces have a considerably higher bending stiffness than the void parts, resulting in wave scattering. In 2020, Kirchhof et al. [48] explored tuning of microscale PCs via applied mechanical pressure. The pressure applied shifted the PC's BGs to higher frequencies.

In PCs, similarly to the photonic crystals, the BGs are originated from the high impedance contrast between the periodic inclusions and the hosting medium. Bragg scattering, a phenomenon of destructive interference between incoming and scattered waves, happens for wavelengths corresponding to the characteristic periodicity length scale, leading to wave propagation attenuation through the complex medium for these frequency ranges. As expected, in order to create BGs at low frequencies, the characteristic periodicity length of the PC must be high. This fact implies the need for huge and bulky structures.

1.3.2. Locally Resonant Metamaterials

At the begging of the millennium, a new solution to control vibration and noise was introduced, the locally resonant metamaterials (LRMs). The establishment of BGs at low frequencies with PCs implies that the characteristic periodicity length of the PC must be high, enforcing the creation of large structures. This reality can be an obstacle in a lightweight design. On the contrary, the BGs of LRMs are not created by the structure's periodicity, but by the sub-sized resonators' dynamic behavior, which create a Fano-type interference of their reverberated waves on the primary waves [49]. LRMs' UC size and the spacing between the UCs are not required to be of the same order of the wavelength to target. This fact allows the LRMs to prevail over PCs in engineering applications to attenuate low-frequency vibration. Often LRMs are referred by different nomenclature such as sonic crystals [50, 51, 52], locally resonant sonic materials [53, 54], acoustic metamaterials [13, 55], elastic metamaterials [56, 57] or even locally resonant phononic crystals [58].

The concept of using negative material properties to manipulate electromagnetic waves was first introduced by Veselago in 1968 in the field of electromagnetics [59]. However, since naturally occurring materials do not exhibit negative material properties, it wasn't until the turn of the millennium that a more practical study on the subject was conducted by Pendry et al. in 1999 [60]. Their study demonstrated that microstructures made of nonmagnetic conducting sheets could exhibit effective magnetic permeability, which can be adjusted to values not achievable in naturally occurring materials. Unlike the previous approach relying on Bragg interference, this new approach utilized resonances of the microstructure for wave manipulation at a specific frequency [60]. This concept was later applied to the field of vibroacoustics by Liu et al. [53] and Sheng et al. [54]. They achieved a higher sound transmission loss compared to the conventional mass-density law of sound transmission by constructing an LRM consisting of small metallic spherical inclusions coated by a thin uniform layer of silicone rubber in an epoxy matrix. The system induced BGs associated with the inner resonances of the arrangement. Negative effective mass density for the elastic wave propagation was achieved in these frequencies regions [54, 9]. This pioneering approach opened the path to the modern research of metamaterials in the field of vibroacoustics. The concept were expanded in other works [49, 61, 62] to different material combinations and geometry. Some works also focused on the description of negative effective mass density by analytical models [63, 61]. Li et al. [64] studied and demonstrated theoretically the concept of double-negative acoustic mediums, which simultaneously have negative effective bulk modulus and effective negative density. Calius et al. [65] and Wester et al. [66] performed additional experiments on this topic. Sample panels with inner small resonating elements were experimentally tested in impedance tubes. The two obtained minimum values for the sound transmission loss (STL) correspond to the two natural frequencies of the partition-resonators systems. The first mode involves the joint movement of the partition and resonator masses, and the second mode involves the out-of-phase movement of the two masses in

opposite directions. As theoretically expected, the transmission loss peak occurred at the anti-resonance, where the two modal contributions to the motion of the partition roughly cancel. The influence of the composite properties, such as the filling fraction and the inclusions' radius, in the BGs was assessed for periodic square arrays of lead discs [67]. Still regarding LRMs with spherical inclusions, Comi et al. [68] conducted numerical studies and demonstrated that hexagonal lattices were more effective in wave filtering than traditional square lattices in two dimensions. Specifically, the dispersion spectrum for the hexagonal lattice exhibited a significantly larger BG than that of the square lattice. The authors also evaluated various combinations of materials for the inclusions, fillers, and external frame.

Vibro-acoustic LRMs take diverse shapes and can be based on different resonating mechanisms. They can be LRMs with resonating inclusions, as previously mentioned; they can be membrane-type LRMs; they take the form of beams or plates with micro-resonators attached; there are even acoustic C-shaped LRMs. For example, Hu et al. [69] presented an acoustic C-shape LRM based on Helmholtz resonance. Comparisons were made between this LRM and an arrangement of rigid cylinders for the creation of acoustic lens, concluding the proposed acoustic C-shape LRM exhibit higher acoustic wave focusing characteristics.

A great number of LRMs mentioned in the literature consist of beams and plates with attached micro-resonators, where the micro-resonators can assume many different forms. Wang et al. [70] investigated the propagation of longitudinal elastic waves in slender beams with harmonic oscillators periodically attached. Similarly, Liu et al. [71] examined the flexural wave propagation in beams with periodic geometric changes, assessing the effects of periodicity on the frequency band structure. In another study on LRM beams, Xiao et al. [72] investigated flexural wave propagation and vibration transmission in LR beams consisting of a periodic array of vibration absorbers attached to a uniform beam. Additionally, they presented a design for LRM beams using periodic arrays of beam-like resonators attached to a thin homogeneous beam [73]. Claeys et al. [74] compared the attenuation achieved for interference BG and resonance BG in Euler-Bernoulli beams and in plates. They explored the importance of the spacing between tuned resonators to define their resonance frequency, as a mean to obtain global vibrational attenuation. The authors demonstrated that the spacing between resonators should be smaller than half of the infinite plate propagation wavelength to achieve relevant vibration attenuation. Moreover, they provided evidence that mass addition is ineffective in creating BGs, as a large amount of mass is needed to obtain a complete BG.

Regarding LRM plates, Wu et al. analyzed the dispersion relation of Lamb waves in plates with periodic circular stubs in the surface [75]. Through numerical and experimental studies, they noticed complete BG forms as the stub height reaches about three times the plate thickness. In 2011, Oudich et al. [58] studied an LRM composed of a periodic arrangement of silicone rubber stubs deposited on a thin aluminum plate. Also, through numerical and experimental studies, they discovered a complete BG for the out-of-plane Lamb wave modes

propagating in various samples fabricated with different stub heights. The authors also refer to the simplicity of manufacturing the proposed structures. In the following year, by the addition of tungsten masses on top of the silicone rubber stubs, Badreddine Assouar et al. [76] achieved a widening and a shift of the toward lower frequencies of the complete BG. The BG transition to lower frequencies is due to the tungsten cap on the stubs acting as a highly concentrated mass that shifts the eigenmodes of the stubs towards lower frequencies. Xiao at al. [77] investigated analytically and numerically the flexural wave propagation and vibration transmission in an LR thin plate with a 2D periodic array of attached spring–mass resonators. In 2014, Claeys et al. [78] continued investigating the topic and provided guidelines for BG design in this type of LRM. They also focused on reducing the acoustic radiation from a structurally excited plate using small mass-spring resonators. It was also concluded that a BG applied at or above the coincidence frequency of the plate reduces the total zone of efficient acoustic radiation. In that year, Xiao et al. [79] proposed a design of LRM consisting of a periodic array of beam-like resonators with their center attached to a thin homogeneous plate, obtaining a complete BG for flexural plate waves. The BGs of this LRM can be tuned by changing the thickness and length of beam-like resonators. Additionally, they remarked that the proposed structures can be fabricated using a single metallic material, which can facilitate its manufacturing and furthermore increase the metamaterial's durability in harsh environments. Hall et al. [80] introduced the idea of multi-layer LRM structures for acoustic barriers. Li et al. [81] studied the effective dynamic properties of these metamaterials. In [82], an LRM metamaterial combined in double-panel structures with poroelastic cores was presented to improve acoustic insulation.

As a remark, another system analogous to LRM discussed in the literature is the multiple tuned mass damper (MTMD) system. For example, in a study by Li et al. [83], MTMD arrangements were examined as a means of reducing unwanted vibrations caused by ground acceleration. These arrangements consisted of several tuned mass dampers (TMDs) with a uniform distribution of natural frequencies, and the researchers investigated various combinations of stiffness, mass, damping coefficient, and damping ratio in each MTMD system. The structures were modeled as single-degree-of-freedom systems. In [84], Bachy et al. highlighted the main difference between MTMD systems and LRMs. They mention that an LRM can be considered an MTMD configuration on a smaller scale. The main difference between the two concepts is the number and size of the resonant structures. LRMs are constituted by a higher number of smaller resonant structures, which allow the reduction of mass of each resonant structure and reduce the space required for its application. According to Bachy et al. [84], multiple studies on vibration energy absorption indicate that multi-structures with distributed vibration absorbers, such as MTMD configurations and LRMs, are more effective at attenuating frequency broadband than traditional TMD configurations.

In the literature, there are also some realizations of membrane-type acoustic metamaterials [85, 86], combinations of membranes with the Helmholtz resonators [87] and introduction of membranes in honeycomb sandwich structures

[88]. In [85] Yang et al. presented a membrane-type acoustic metamaterial to reach nearly total reflection at the frequencies in between two eigenmodes. The researchers continued investigating this type of metamaterial, demonstrating a broadband sound shield comprising simple stacking of membrane-type metamaterials operative over different frequency regimes [86]. Zhang et al. [89] provided an analytical approach for fast calculating STL of the membrane-type acoustic metamaterials. The researchers found the first STL valley and the STL peak are heavily influenced by the mass attached to the membrane, whereas the membrane properties have a greater impact on the second STL valley. Langfeldt et al. [90] investigated the STL through membranes with arbitrarily shaped masses. The same authors proposed a new analytical model for predicting oblique incidence STL of baffled panels with multi-celled membrane metamaterial [91]. In their publication, Kumar et al. [87] describe a metastructure that utilizes double negative material properties to absorb low-frequency noise emissions from aircraft. The metastructure developed by Kumar et al. [87] comprised of hexagonal cells arranged in a periodic array, with interconnecting necks that acted as Helmholtz resonators. Thin elastic membranes were mounted on both ends of the cells, enabling the achievement of negative mass density through in-phase membrane movement. Meanwhile, the combined effect of out-of-phase acceleration of the membranes and Helmholtz resonator resulted in a negative bulk modulus. Li et al. [88] published an article proposing a lightweight multilayer honeycomb membrane-type acoustic metamaterial. The introduction of the membranes on the honeycomb cell enhanced the STL. While the peaks and dips of the structure remain largely unaffected, the researchers noted that increasing the membrane thickness can enhance the overall sound transmission loss (STL) of the metastructure.

Regarding the numerical simulation of LRMs, Krushynska et al. [92] cautioned that the accuracy of predictions based on 2D simulations of 3D LRMs depends significantly on the shape of the resonators in the LRM. In order to achieve accurate predictions for certain designs through numerical simulations, it is necessary to use 3D finite element method representations. Meanwhile, Van Belle et al. [93] have conducted a study on LRM and PC plates, in infinite and finite configurations. They concluded that the presence of structural modes in the finite case can affect the prediction accuracy of the STL performances.

Few works focus on translating the LRM academic developments to practical applications. When it comes to engineering applications, there are additional criteria that must be met. It is crucial to identify LRMs that can meet other functional requirements, including structural integrity, shielding from contaminated environments, and providing adequate thermal conductivity. Claeys et al. [94] suggested a design of sandwich panels with resonators added into the internal cavities, several resonator distributions and their BGs were studied. To numerically simulate the LRM demonstrator, Claeys et al. decoupled the structural model and the acoustic model, enabling the structural mesh to be very refined while the acoustic model had a coarser mesh.

Melo et al. [10] and Claeys et al. [11] analyzed a square cross-section PVC duct that contained resonant structures arranged in different configurations,

including those with two kinds of tuned resonators, each resonating at different frequencies. The aim of the research was to investigate the production of BGs in the frequency range where the resonant structures were tuned. The researchers used two different UC modeling approaches: the direct approach for 1D UC analysis, which considers the effects of the duct's geometry, and the inverse approach for 2D UC analysis. The results of the studies showed that the resonant structures did indeed produce BGs in the frequency range where they were tuned. The experimental results confirmed these findings. Furthermore, the research revealed that increased damping led to a less pronounced peak attenuation but widened the range of the BG.

Sangiuliano et al. [95] introduced an application case of LRMs to reduce the vibration of a simple plate structure subjected to a frequency-dependent force. The objective of the created metastructure was to prevent the amplification of vibration levels by the structural modes. Small resonators made of polymethylmethacrylate (PMMA) with a steel mass attached were bonded to the plate structure. Yu et al. [96] proposed a resonant structure that could be incorporated into plates to reduce noise and vibration in industrial applications. The resonant structure was made of acrylonitrile butadiene styrene (ABS) for the spring part and steel for the mass part, and was manufactured using injection molding with the metal part already in place. This ensured permanent attachment between the plastic and steel components, providing a solution for the manufacturability of locally resonant structures in mass production. The authors verified that the metamaterial structure exhibited higher vibration reduction in the target frequency band compared to other conventional NVH solutions.

The first application of LRMs to industrial automotive structures was reported by Jung et al. [97]. The authors attached small tuned resonators to an automobile dash panel structure and measured its acoustic and vibration responses. The resonators were attached to the host part using a permanent magnet, enabling the application to more complex surfaces without any structural changes. The authors examined the vibration response and the acoustic response. However, they observed some discrepancies between the numerical and experimental results, which were attributed to the lack of periodicity in the experimental setup assumed in the numerical analysis and the coupling of flexural and in-plane waves on the curved surface of the dash panel, weakening the effect of the local resonators. Broadband reductions in surface velocity were observed. Comparing the vibration and the acoustic response, it was concluded that there was an increase in the radiation efficiency, caused by vibration concentration in some areas, leading to piston-like radiation of acoustic waves. This increase in radiation efficiency was previously discussed by Claeys et al. [78] for the case of an LRM flat plate, where the introduction of resonators in the plate increased the radiation efficiency in frequencies just above the BG due to a coincidence effect of the acoustic wave. To mitigate this issue, the authors suggested introducing a material with high damping in the vibration concentration area. Despite these challenges, the measurement results demonstrate a significant reduction in vibration and noise radiation from the dash panel structure in the

defined BGs [97].

Droz et al. [98] conducted a study on the effects of tunable resonators on the sound transmission loss (STL) of an aircraft sidewall panel under diffuse acoustic field excitation. The tunable resonators used in the study were 3D-printed cantilever beams with interchangeable tip-end magnets. The study considered different spatial arrangements of the resonators, including multi-resonant configurations and the combination with other sound-absorbing treatments. Chang et al. [99] presented a study on improving automobile acoustic insulation pads using LRMs. They incorporated a metamaterial layer into the insulation pad to enhance its performance in reducing sound transmission, while also reducing the thickness of the isolation and absorption layers to decrease the pad's weight. The effectiveness of the LRM-enhanced insulation pad was tested on a vehicle firewall. In the same year, Sangiuliano et al. applied LRM metamaterials to the rear shock towers of a vehicle [100]. The metamaterial configuration showed similar or better performance in reducing noise, vibration, and harshness (NVH) compared to the currently used tuned vibration absorber (TVA) configuration. Moreover, it reduced the added mass of the NVH solution by 48%, making it a more lightweight option.

In order to optimize the BGs of metamaterial structures, several approaches have been proposed in the literature, including those by Yang et al. [101], Chen et al. [102], Kook et al. [103], Wormser et al. [104], and Han et al. [105]. Van Belle et al. [106] developed a fast design optimization process for 3D UC metamaterials to attenuate bending waves. Their metamaterial UC design creates a BG for bending waves by utilizing the first out-of-plane bending mode of the micro-resonator. To expedite the process, they used a reduced-order UC modeling for predicting the size and frequency location of the BGs. They observed that the optimization tends to maximize the allowed mass ratio (defined in the design constraints) since an increase in the mass of the micro-resonators increases the BG size [74, 106]. Furthermore, the optimization process tends to minimize the base dimensions (length and height) of the micro-resonators. Pires et al. [107] conducted a study on the impact of micro-resonator footprint size on their performance. According to their results, utilizing smaller footprints lead to wider BGs. Thus, it is recommended to employ micro-resonators with the smallest possible footprint, as long as a reliable connection to the host structure is maintained.

Elias and Matsagar [108] published a review on the developments in vibration control of structures using passive resonating systems, where it can be noticed that the research in the optimization of the multi-resonator distributions and its characteristics was not in a mature state. In 2018, Kim et al. [109] progressed in the optimization of multiple linear TMDs in one dimension, defining a method to set the different dynamic characteristics of each TMD. Some other methodologies for the optimization of MTMDs can be found in the recent literature, for example Vellar et al. [110] defined a method for optimization of MTMDs' design parameters and their best positions over the buildings subjected to earthquakes. Americano da Costa et al. [111] proposed a process to optimize the design of spatially distributed TMDs to minimize system responses while considering up-

per bounds for damping ratios. They concluded that the TMDs parameters and distribution highly depend on the considered damping ratios. Their process starts with defining a single TMD design and sequentially moves to a set of TMDs organized in series and finally moves to a group of spatially distributed TMDs with different characteristics. Despite recent progress, studies on optimizing multi-resonator systems have highlighted the high sensitivity of these optimizations to various factors, such as input parameters and uncertainties in material damping. Additionally, the objective function used in optimization must be tailored to the specific application objective. As shown in the works of Zouari et al. [112], the change of the mechanical parameters for the resonator varies the limits of the BGs. Also, due to variability in additive manufacturing, detuned resonators can change the attenuation performance, affecting the BGs in real applications [113, 114]. In [84], Bachy et al. state that traditional lumped mass models still need to be enhanced in order to consider the real topology of the elements in metastructures. They also highlight the effects of uncertainties in quantifying damping performances of resonating structures in different environmental conditions, aging of materials and assembly conditions.

1.3.3. Metamaterial Solutions for application on GBHs

Since the LRMs do not depend on the periodicity of the arrangement and the resonating structures are sub-wavelength sized, their implementation is more feasible in engineering applications, especially in the low-frequency region where the wavelength is higher. Moreover, the resonating structures can be tuned to reduce the vibration and noise emission in distinct frequency zones. For these reasons, LRM solutions can be a mean to reduce the noise emission from the GBH while maintaining a lightweight and compact design, and give a particular emphasis to LRMs physics and their modeling. Noise reduction is crucial to complying with the set noise rules and ensuring the highest possible acoustic comfort for the individuals inside and outside the vehicles.

As stated in this review, some automotive metamaterial solutions can be found in the recent literature, although to our knowledge, there is no application of these concepts to GBHs neither to EV motor housings. It is worth noting that modern EV motor housings and GBHs both enclose geared systems and share similar structures and functionalities. In fact, currently, they are often manufactured by the same companies. Therefore, solutions developed for GBHs can also be adapted and applied to EV motor housings.

Industrial manufacturers have tight deadlines to bring new products to market, which can make optimizing the design of metamaterials challenging. The reviewed literature suggests that the process of optimizing metamaterial designs is complex, particularly in real-world applications where design complexity and uncertainties present significant challenges. As a result, the optimal design solutions may be too difficult and time-consuming to implement in industrial processes.

Another important point raised by the manufacturers is the housing manufacturing cost. Production costs are a relevant factor in the industry, for that reason it is important to consider cost implications when developing solutions

for automotive components. Any proposed solutions should aim to minimize additional costs and ensure that they are economically viable for manufacturers to implement.

As a result, it may be worthwhile to explore whether even fast design LRM solutions can provide benefits in application in GBHs by improving their NVH behavior and enabling lightweight design. While they may not provide the maximum possible benefit, even suboptimal solutions could still offer significant improvements and be more practical for industrial implementation within the given time and cost constraints.

2. Material and Methods

2.1. Considered GBH Geometry

The design of gearbox housings (GBHs) is often complex and can be greatly affected by the arrangement of internal components, external connections, and auxiliary parts such as actuators and electric units. This can result in intricate structures with numerous openings, connections, patterns, and thickness variations on the surface. The starting GBH design considered in this investigation was a simplified gearbox housing geometry based on the works of Figlus et al. [115, 116], focusing solely on the top part of the GBH to simplify the analysis. This approach streamlines the study while still providing valuable insights into the behavior of GBHs.

2.2. GBH Loading for Numerical Studies

The mechanical loading at the GBH's bearing connections depends on the rotating components' geometries, characteristics, and assembly configurations. The mechanical loading depends, in particular, on the transmission ratio, the inclination angle of the gear teeth (in the case of helical gears), the transmitted power, the input speed, and the distance between axes [1]. At the bearing support, loads are transferred from the shafts to the housing structure in radial and axial directions. In this work, a typical characteristic loading was applied in the GBH bearings'connection in the bearings areas according to Figure 1. A simple gearbox with helical gears was a reference for the bearing's loading. Figure 2 displays the loading for each of the four bearing connection regions.

2.3. Experimental Validation Details

An aluminum alloy (AA7075) housing was manufactured for experimental validation of the LRM solution concept for attenuation of low-frequency peaks and broadband vibration attenuation; see geometric details in the appendix Appendix B. The manufactured housing is designed with an M4 bolted connection between the top plate and the main structure, allowing the interchangeability between the baseline configuration and LRM solution configurations in the GBH.

Figure 3 shows the idealized experimental stand. The mock-up GBH was connected to the experimental stand by a bolted connection (14xM6 bolts -

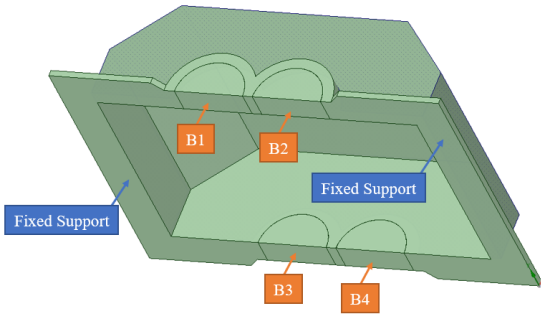

Figure 1: Location of the excitation for each bearing: Bearing 1 (B1), Bearing 2 (B2), Bearing 3 (B3), Bearing 4 (B4); and the Fixed Support Boundary Conditions.

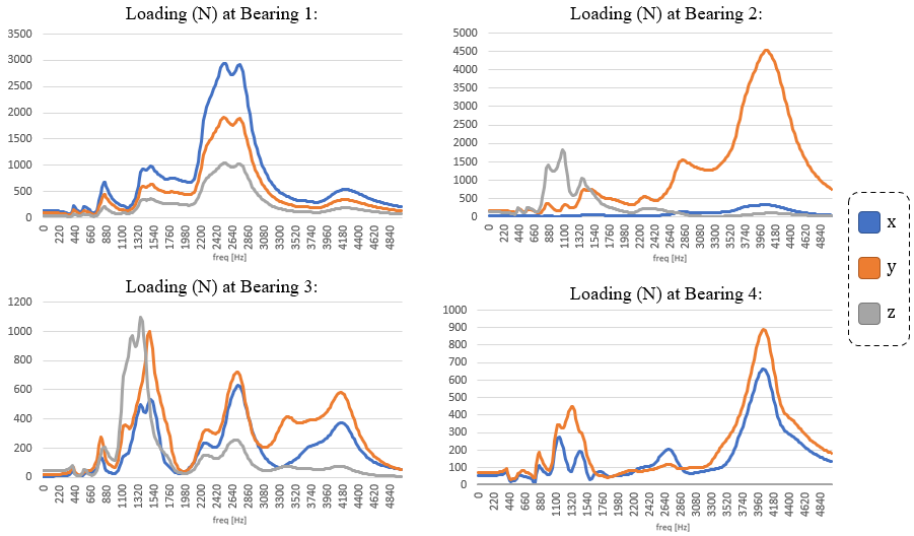

Figure 2: Loading for each of the four bearings in x (side), y (upwards) and z (axial) directions.

torque 5.4 Nm). The input force in the mock-up GBH was generated by an electrodynamic shaker Robotron 11076 connected to a 3 mm diameter stinger (400 mm long). The input force was applied in the middle of the bearing's region and was measured by a PCB Piezotronics ICP dynamic force sensor between the stinger and the mock-up GBH. The top plate was bolted to the GBH top flange using 18 M4 bolts (torque 1.6 Nm). The acceleration was measured in 7 positions of the GBH, according to the Figure 4, using 7 accelerometers sensors (1 triaxial accelerometer sensor I-TEDS model-66A12 and 6 uniaxial accelerometer sensors type 4508-B-002) connected to 2 acquisition units Bruel & Kjaer Type 3050-A-060 connected to an ethernet switch Cisco SG300-10MP Managed Switch. The signal time recording was made using Bruel & Kjaer Pulse Recording software, using a 6.4kHz frequency range. The signal processing and post-processing were made using Bruel & Kjaer Pulse Reflex software and MATLAB.

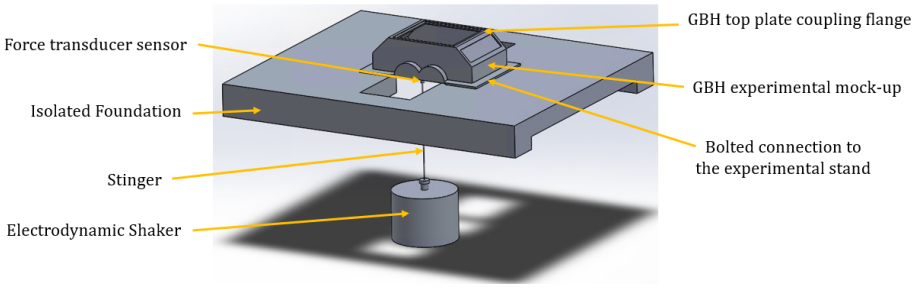

Figure 3: 3D illustration of the experimental setup.

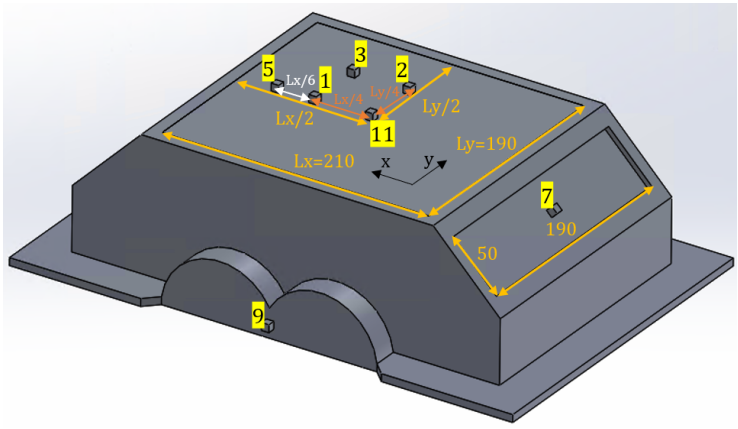

Figure 4: Accelerometer sensors positions on the GBH (dimensions in mm).

3. Theory and Calculations

3.1. GBH Lightweight Design

The basis of lightweight design is to reduce the mass of a structure while ensuring that its functionality is not compromised. Topology optimization methods are valuable in achieving this objective, enabling the multi-objective optimization of the housing geometry. As mentioned before, there are some works on the subject of structural optimization of GBHs in the literature that use topology optimization methods [1, 2, 3]. In this study, the original GBH's mass was decreased using a similar topology optimization approach, which optimized the material distribution within the predetermined design space. The goal of the optimization process was to minimize structure compliance, maximizing structural stiffness. Material was removed from locations that contribute less to the overall stiffness of the GBH following the topology optimization process. Figure 5 illustrates the process for the considered GBH. The thickness of the top plate and the side plates was reduced from 6 mm to 2 mm, generating a lightweight version of the GBH. In this work, the two GBH versions are considered, the original GBH and the lightweight version of the GBH. The mass of the lightweight GBH is 6.81 kg compared to the 8.92 kg of the original steel GBH, which is a 24% relative mass reduction. If we consider the inclusion of bearings parts, the total mass of the original GBH is 10.98 kg, while the total mass of lightweight GBH is 8.87 kg, which represents a 20% relative mass reduction.

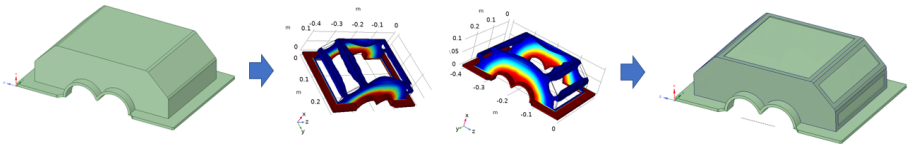

Figure 5: Illustration of the followed topology optimization process.

3.2. Initial Sound Power Radiated Assessments

The sound power radiated, over the frequency domain, is obtained by integrating the far-field intensity over a hemispherical surface centered on the structure [6], as written in Equation 1. Sound Power Levels are indicated in decibels, by the following formula stated in Equation 2, where the reference power $P_0 = 10^{-12}W$.

$$P_{radiated}(\omega) = \int_S I(\theta, \phi, \omega)\, dS = \int_0^{\pi/2} \int_0^{2\pi} I(\theta, \phi, \omega) r^2 sin(\theta)\, d\theta\, d\phi \quad (1)$$

$$L_w = 10 \cdot log\left(\frac{P_{radiated}(\omega)}{P_0}\right) \quad (2)$$

A comparison of the sound power radiated from the original GBH and the lightweight GBH was conducted by numerical simulations, as shown in Figure 6.

The numerical simulations were performed in the commercial software COMSOL Multiphysics (version 5.6). The model was solved in the frequency domain using the solid mechanics and pressure acoustics modules, with an acoustic-structure boundary within COMSOL Multiphysics. The properties of the considered steel material are the following: Density of 7850 $[kg/m^3]$, Young's modulus of 200e9 $[Pa]$, Poisson's ratio of 0.3 and isotropic structural loss factor of 0.1%. A hemispherical acoustic air domain of 0.4 m radius was set around the GBH. The considered air material properties depend on the ambient pressure p_A and temperature T. The speed of sound c and the density ρ are defined through the ideal gas law (assuming adiabatic behavior), according to Equation 3 where R stands for universal gas constant ($R = 8.3144621[J/(molK)]$), γ stands for the ratio of specific heats ($\gamma = 1.4$) and the M_n is the molar mass $M_n = 0.02897[kg/mol]$. The considered ambient pressure and temperature were 1 atm and 20$^{\text{o}}$C (293.15 [K]), respectively.

$$c^2 = \gamma \frac{R}{M_n} T \qquad \rho = \frac{M_n p_A}{RT} \tag{3}$$

A Perfectly Matched Layer (PML) was set between the radius of 0.35 m and 0.4 m to represent the open environment [117]. The maximum element size was set as the speed of sound divided by five times the highest frequency to be modelled. The structural-acoustic model for the original GBH was constituted by 810509 elements, with an average and minimum quality of 67% and 18%, respectively. The lightweight GBH model was comprised of 852208 elements, with an average and minimum quality of 65% and 14%, respectively. The integration of the sound power radiated was made at a radius of 0.3 m. The model structural loading was the bearings' loading described in Figure 2, and its application was made in the geometry areas stated in Figure 1. A fixed support was considered in the connecting interface to the other half of the GBH, as shown in Figure 1.

As visible in Figure 6, the mass reduction changes the frequency location of the sound power radiation peaks. It is also perceptible by the housing deformation shapes that the sound power radiated peaks generally correspond to the eigenmodes of the structure, most of them corresponding to the local eigenmodes of the top plate. It is particularly important to note that reducing the mass of the GBH results in the appearance of a peak at 425 Hz, which corresponds to a shift in the first local eigenmode of the top plate. In order to normalize the power results, the sound power radiated results were divided by the power injected into the structure. The total power injected is calculated by the summation of the power injected in each bearing, see Equation 4. The power injected for each bearing is calculated according to the integral over the area of load application stated in Equation 5, where f and v denote the applied force and velocity complex amplitudes in the loading area, respectively, and ^{H} is the complex transpose conjugate operator [118]. The ratio of the sound power radiated to the power injected in the structure, see Equation 6, is depicted in Figure 7 for the original GBH and the lightweight GBH. For the sound power

radiated, it is possible to see the same trend in both the nominal and normalized results.

The goal of this research is to create innovative and lightweight GBH designs with desirable NVH characteristics. As mentioned previously, recent advancements in the field of metamaterials can offer potential opportunities to leverage the NVH characteristics of GBHs. The upcoming chapter will focus on exploring simple and cost-effective LRM solutions for application in GBHs.

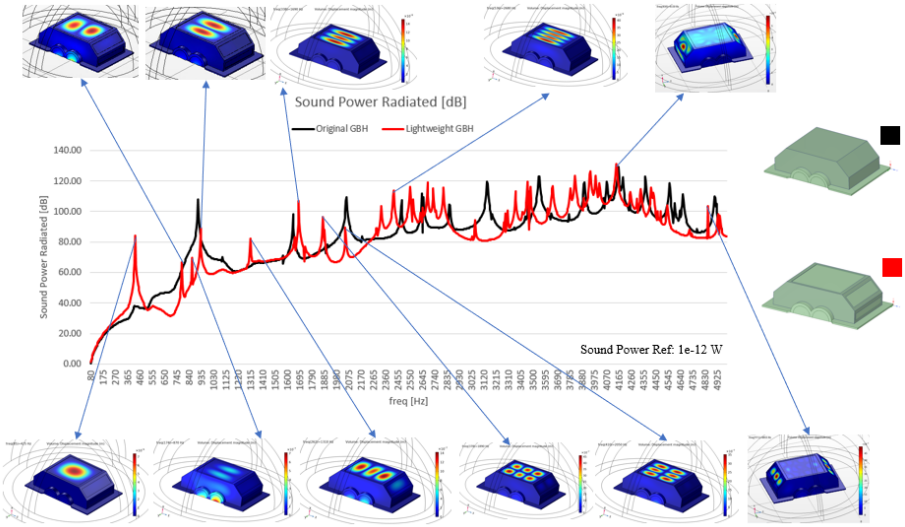

Figure 6: Sound power radiated comparison between the original GBH (black) and the lightweight version of the GBH (red), complemented with a number of housing deformation shapes.

$$P_{injeted\,total}(\omega) = P_{injeted\,B1}(\omega) + P_{injeted\,B2}(\omega) + P_{injeted\,B3}(\omega) + P_{injeted\,B4}(\omega) \tag{4}$$

$$P_{injeted}(\omega) = \frac{1}{2}\int_A \Re e\{v(\omega) f(\omega)^H\}\, dA \tag{5}$$

$$PowerRatio(\omega) = \frac{P_{radiated}(\omega)}{P_{injeted\,total}(\omega)} \tag{6}$$

3.3. GBH Locally Resonant Metamaterial Solutions

As emphasized in the literature review, it is challenging to attenuate low-frequency peaks such as the one observed at 425 Hz using traditional noise and vibration reduction techniques [119]. One promising approach to address this challenge is by introducing vibroacoustic LRMs. Thus, this section investigates

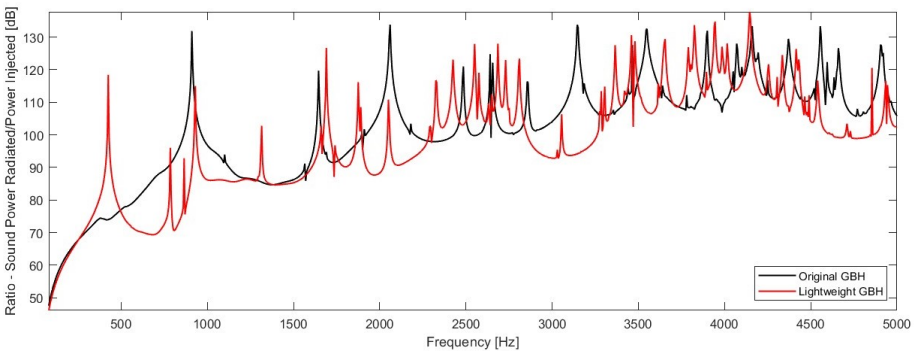

Figure 7: Ratio between the sound power radiated and the power injected in the structure of the original GBH (black) and the lightweight GBH (red).

simple and cost-effective LRM solutions that can enhance the NVH characteristics of GBHs.

The initial step of the study was to determine the appropriate location for applying the LRM (Locally Resonant Metamaterials) solution. As demonstrated in Figure 6 and Figure 7, the sound power radiated peaks in the lower frequency region are caused by the vibration of the top plate of the lightweight GBH. Therefore, in this study, an LRM solution was applied to the top plate to reduce the vibration at these frequencies. Similarly, in more complex industrial GBHs, it is crucial to apply the LRM solutions in positions where the vibration levels are high at these low frequencies, typically corresponding to areas with lower stiffness.

Due to the simple geometry of the considered GBH, it is possible to clearly identify the mode shape of the corresponding peak at 425 Hz, which corresponds to the first local eigenmode of the top plate. So in this specific case, it would be possible to optimize the LRM mass distribution over the top plate (for example, mass concentration in the plate center). However, in an industrial GBH, optimizing the LRM mass distribution would not be a simple task, as highlighted in the literature review. For that reason, a constant mass distribution LRM solution was employed in this study to showcase that simple and fast design solutions are possible to be introduced in the GBHs, without spending excruciating time in the design phase and without reaching highly complex LR distributions, which would entail high costs. Even though it is known a priori that the LRM solution might be suboptimal.

As seen in the LR metamaterial literature review, the LRM solution is expected to provide not only the useful attenuation in the low-frequency region where they are tuned to, but also a considerable broadband attenuation. The broadband attenuation is originated from the structural damping associated with the LRM [73, 120, 74, 119].

For the first LRM solution to be applied in the lightweight GBH, a UC size of 20 mm x 20 mm was considered. Given that the top plate dimensions are 204

x 190 mm, it is possible to fit 90 UCs in a rectangular pattern. The bibliography contains several distinct types of micro-resonator designs with various geometries and resonant mechanisms [121, 11, 112, 95, 96, 98, 99, 100]. In this case, a simple micro-resonator geometry was considered, based on the same resonant mechanism of the micro-resonators presented in [11, 95, 96, 98, 99], see Figure 8. The micro-resonator consists of an acrylic part and a steel mass on the top. The up-and-down vertical movement of the micro-resonators mass will dynamically absorb the vibrational energy of the host structure, dampening the bending waves on the structure. The acrylate polymer material properties considered in this study are the following: Density of 1190 $[kg/m^3]$, Young's modulus of 3.2e9 $[Pa]$, Poisson's ratio of 0.35 and isotropic structural loss factor 5%. Even for a micro-resonator with a simple geometry, there are several design variables to be controlled [121, 122, 112]. For this micro-resonator design, several dimensional parameters must be defined, such as its width, the length/thickness of the flexible part and the dimensions of the mass part.

The proposed resonating UC has two main advantages. First, it is prone to application on the outside of the GBH without requiring a structural redesign, making it a viable solution for dealing with specific NVH problems encountered even during the final stages of industrial design. The second advantage relates to its easy frequency tuning. The frequency tuning of a micro-resonator is performed using the relation between the natural frequency and parameters of a vibration system. The micro-resonator spring part affects mainly the stiffness (k), and the concentrated mass part affects the mass (m). The following methods can be used to decrease the stiffness of the micro-resonator: decrease the thickness of the micro-resonator spring part; increase the length of the micro-resonator spring part; change the shape of the micro-resonator spring part, for example, by the inclusion of slits in the micro-resonator spring part. Opposite methods can be used to increase the stiffness of the micro-resonator. The mass of the micro-resonator can be adjusted simply by changing the concentrated mass (changing the mass dimensions or changing the material). Using these relations, it is possible to tune the frequency band where the vibration is highly attenuated.

Jung et al. [97] and Claeys et al. [94] stated additional properties that an LRM should have in practical engineering applications, for example, its manufacturability, its compatibility, and its sub-wavelength scale characteristics. Regarding manufacturability, the proposed micro-resonator spring part can be manufactured by 3D printing/additive manufacturing, and the mass part of the micro-resonator can be bonded to the spring part by adhesive bonding. The micro-resonator design can also be easily adapted for mass production, as shown in 2019 by Yu et al. [96]. The resonator was designed by changing its dimensions within the design limits, taking into consideration the following objectives:

1. Tuning the first eigenfrequency (bending mode) of the micro-resonator to the desired hard-to-tackle low frequency;
2. Maximize the ratio of the modal mass for the micro-resonator's first eigenmode by the total mass of the micro-resonator;

3. Minimize the nonessential mass addition, since lightweight design is the goal, the total mass added by the micro-resonator should be minimized (e.g., minimize the mass of the bending beam part of the micro-resonator).

Aiming for the previously stated objectives, and defining the tuning eigenfrequency of 425 Hz, a micro-resonator width of 16 mm was defined, the acrylic base was defined as a square cross-section of 4×4 mm, the acrylic beam was defined with a thickness of 1 mm and a length of 14.547 mm, and finally the steel mass was defined as a square cross-section of 4×4 mm.

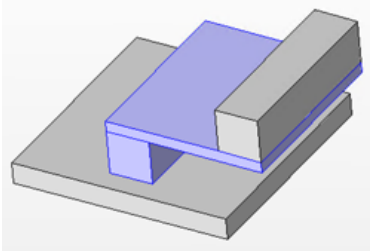

Figure 8: UC with micro-resonator: acrylic part (blue) and steel part (grey).

Even though Locally Resonant (LR) structures can be applied in non-periodic ways, striving to simplify the analysis of LRMs in the majority of the cases in the current literature, assume an infinite periodic distribution of LR structures [123, 62, 53]. This way, a complete representation of the LRM can be obtained using a UC and Floquet–Bloch boundary conditions. Figure 9 shows a schematic representation of a two-dimensional periodic structure. The periodic structure is a repetition of a generic UC in two directions, being $\mathbf{d}_x$ and $\mathbf{d}_y$ the basis vectors of the UC. Given that the structure is periodic, any point P in the structure can be expressed with respect to a corresponding point U in the unit cell, translated n_x cells along $\mathbf{d}_x$ and n_x times along $\mathbf{d}_y$, see Equation 7 [74].

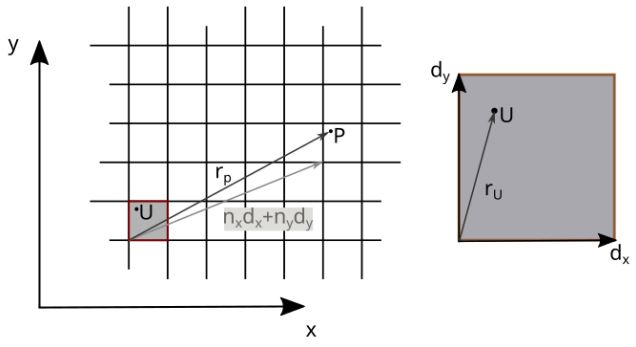

Figure 9: Schematic presentation of an infinite periodic structure (left). A unit cell of the structure (right).

$$\mathbf{r}_P = \mathbf{r}_U + n_x \mathbf{d}_x + n_y \mathbf{d}_y \tag{7}$$

The theorem of Bloch states that the response of a two-dimensional periodic system can be expressed in terms of the response of a reference unit cell. The amplitude and phase change of a wave propagating in an infinite periodic structure may be defined by an exponential term, see Equation 8 [124, 74], where the '$\cdot$' indicated a scalar product.

$$u(\mathbf{r}_P, \omega) = u_{ref}(\mathbf{r}_U, \omega) e^{\mathbf{k} \cdot (n_x \mathbf{d}_x + n_y \mathbf{d}_y)} \tag{8}$$

The wave vector $\mathbf{k} = (k_x, k_y)$ defines the amplitude and phase change. In infinite periodic structures, the propagation vector μ, defined in Equation 9, expresses the complex phase shifts when in motion within a cell in the $\mathbf{d}_x$ and $\mathbf{d}_y$-directions.

$$\mu = (\mu_x, \mu_y) = (\mathbf{k} \cdot \mathbf{d}_x, \mathbf{k} \cdot \mathbf{d}_y) = \mathbf{k} \cdot \mathbf{d} \tag{9}$$

Employing this notation to rewrite the Bloch theorem, Equation 10 is reached, where $\mathbf{n}$ is a vector indicating the amount of cells moved in each direction in relation to the reference UC.

$$u(\mathbf{r}_P, \omega) = u_{ref}(\mathbf{r}_U, \omega) e^{\mu \cdot \mathbf{n}} \tag{10}$$

Using the infinite periodic structure theory allows the study of wave propagation in LRM without the necessity of full-scale finite-structure vibroacoustic numerical models [123, 74]. The distinctive vibroacoustic performance of LRMs is assessed by the presence of BGs in the dispersion curves. Dispersion curves display the relation between frequency and wavenumbers.

For rectangular lattices, the periodic zone in the wave domain, called a Brillouin zone, can be circumscribed in $[-\pi, \pi]$ in both principal directions. Employing the UC symmetries, the area to study can be further reduced in the irreducible Brillouin zone (IBZ). The IBZ depends on the shape and symmetries of the UC [125]. There is a common practice of assessing the abovementioned BGs in the LRM dispersion curves, by the calculation of the dispersion curves exclusively on the IBZ boundaries, also known as irreducible Brillouin contour (IBC) [124, 123, 97]. The most common strategy to study LRM periodic structures is the discretization of the UC using the FE method and the definition of Bloch-Floquet boundary conditions on the UC boundaries to obtain a dispersion eigenvalue problem [99, 98, 94, 96, 95, 11, 97, 126]. This is known as the wave finite element (WFE) method [127, 128, 129]. A similar FE based UC modelling approach was followed in this work.

Generally, there are two modelling approaches to get the dispersion curves. One is the inverse or $\omega(\mu)$ approach in which the real propagation constants μ are defined and the dispersion eigenvalue problem is solved to frequencies ω. And the other is the direct or $\mu(\omega)$ approach which imposes the real frequencies ω and solves the dispersion eigenvalue problem to propagation constants μ [123]. The $\mu(\omega)$ approach is suitable for 1D periodic structures, however its application

to 2D periodic structures is more complicated [123]. In this work, an inverse approach was followed, spanning through the values of k_x and k_y, and obtaining the eigenfrequencies. The Irreducible Brillouin Contour (IBC) was established according to the diagram in the left of Figure 10. An auxiliary variable k was defined, varying from 0 to 4 while spanning all the IBC. For k varying from 0 to 1, the wave vector $\mathbf{k} = (k_x, k_y)$ spans from $(0, 0)$ to $(\pi/al, 0)$, where al is the UC side length. For k varying from 1 to 2, the wave vector $\mathbf{k} = (k_x, k_y)$ spans from $(\pi/al, 0)$ to $(\pi/al, \pi/al)$. For k varying from 2 to 3, the wave vector $\mathbf{k} = (k_x, k_y)$ spans from $(\pi/al, \pi/al)$ to $(0, \pi/al)$. For k varying from 3 to 4, the wave vector $\mathbf{k} = (k_x, k_y)$ spans from $(0, \pi/al)$ to $(0, 0)$. On the right side of Figure 10 the dispersion curves for the LRM UC are shown. The presence of the micro-resonator in the UC introduces discontinuities in the bending wave propagation. A complete BG is found between 425 Hz and 474 Hz, which is created by the up-and-down movement of the micro-resonator mass, which dampens the vibration of the structure and dissipates the vibrational energy.

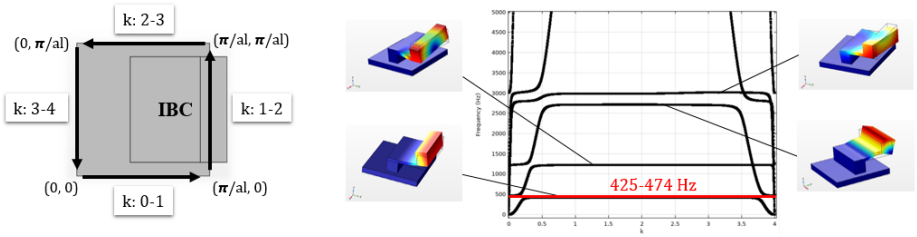

Figure 10: Definition of the Irreducible Brillouin Contour (IBC) for the LRM UC - left; and LRM UC dispersion curves around the IBC - right.

In Figure 11 the lightweight GBH with the LRM solution applied is shown, zoom was made to show the placement of the micro-resonators in the LRM assembly. This first LRM configuration was denominated LRM1. For the purpose of sensing the mass addition quantities, the mass of the original GBH is 10.98 kg (including the bearings part), while the mass of lightweight GBH is 8.87 kg (including the bearings part), which represents a reduction of 2.10 kg (20% reduction). The added mass added from all micro-resonators in this LRM solution is only 0.232 kg (2.6% increase relative to the lightweight GBH mass). The LRM introduction represents a very slight mass addition compared to the previously obtained mass reduction. After applying the LRM solution, the total mass of the lightweight GBH still decreased by more than 17% compared to the original GBH.

A computation of the sound power radiated by the lightweight GBH with the LRM1 solution, subject to the same loading, was made through numerical simulations with the same setup described previously in Section 3.2. The structural-acoustic model for the lightweight GBH with the LRM solution was constituted of 982855 elements, with an average and minimum quality of 64% and 15%, respectively. The results' comparison between the GBH, the lightweight version of the GBH and the lightweight GBH with the LRM solution applied can

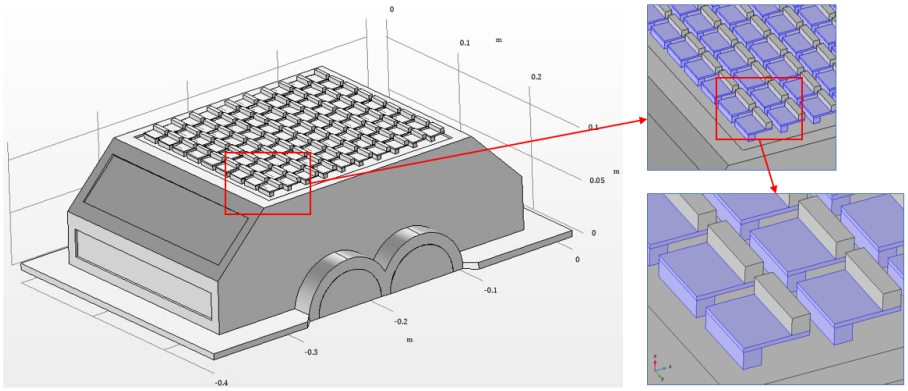

Figure 11: Lightweight GBH with LRM1 solution applied in the top of the GBH.

be seen in Figure 12. The results confirm the attenuation from the predicted BG between 425 Hz and 474 Hz. The introduction of the LRM solution in the housing attenuates the first sound power radiated peak at 425 Hz, a type of attenuation similar to a tuned mass damper (TMD) behavior. The presence of the micro-resonators reduces the original peak at 425 Hz and introduces two other smaller peaks in the vicinity, one at 330 Hz and another at 575 Hz. Moreover, as discussed before, the LRM Solution provides also a broadband attenuation of the sound power radiated over the considered spectrum. A significant reduction of the sound radiation peaks is noticeable in Figure 12.

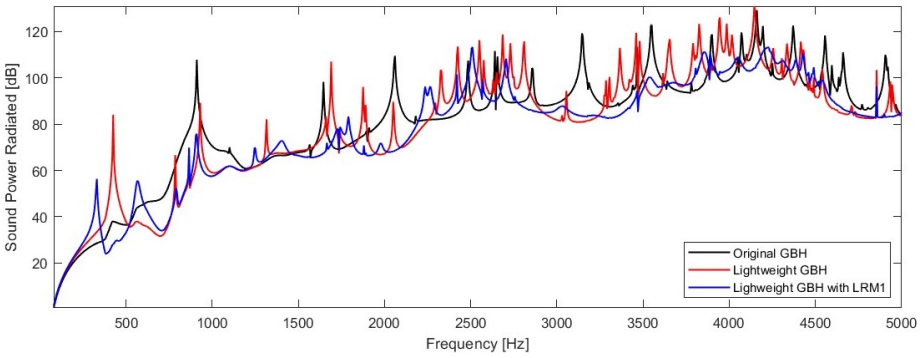

Figure 12: Sound power radiated comparison between the original GBH (black), the lightweight version of the GBH (red) and the lightweight GBH with the LRM1 solution applied (blue).

The ratio of the sound power radiated to the power injected in the structure was also calculated for the lightweight GBH with the LRM solution applied, its comparison with the results from the original GBH and the lightweight GBH depicted in Figure 13. It is possible to observe the same trends in the normalized

results as in the nominal results for the sound power radiated.

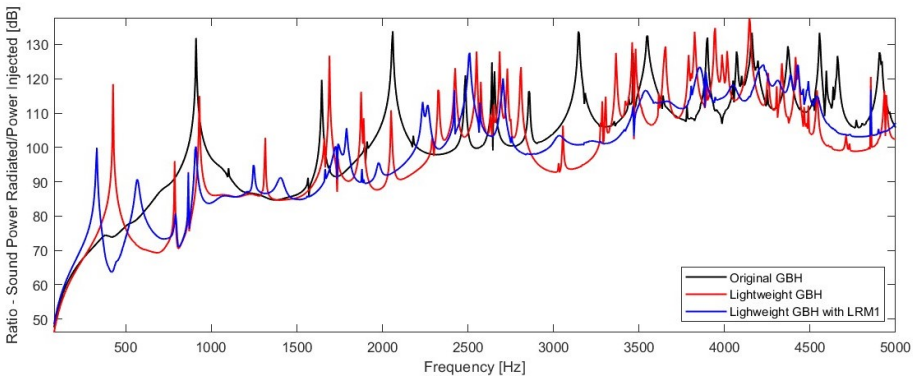

Figure 13: Ratio between the sound power radiated and the power injected in the structure of the original GBH (black), the lightweight GBH (red) and the lightweight GBH with the LRM1 solution applied (blue).

A second LRM solution was idealized (LRM2), consisting of an LRM with two groups of micro-resonators intercalated. One group is constituted by micro-resonators similar to the one already mentioned, see Figure 8. The second group is constituted by micro-resonators with similar geometry but with different dimensions, so that the micro-resonators have their 1st eigenfrequency (bending mode) tuned to another frequency. In this case a frequency of 870 Hz was chosen to create another BG coinciding with the other peaks in the lower frequency. The dimensional changes were the following: the acrylic beam length was changed to 12 mm and the steel mass cross-section was change to 3(length)$\times$ 2.6953(height) mm. Following the same dispersion curve analysis method described previously in this section, the relevant BG is achieved between 870 Hz and 925 Hz. The two groups of resonators were assembled in intercalated lines, see Figure 14. The total mass added with the two groups of the micro-resonators was 0.185 kg, which corresponds to a 2.1% mass increase relative to the lightweight GBH mass.

Another computation of the sound power radiated by the lightweight GBH with the second LRM solution, subject to the same loading, was made through numerical simulations with the same setup described previously. The structural-acoustic model for the lightweight GBH with the second LRM solution was constituted by 975256 elements, with an average and minimum quality of 64% and 8%, respectively. The results can be seen in Figure 15. Comparing both LRM solutions, the LRM solution with two types of micro-resonators combined shows a higher attenuation of the sound power radiated in the frequency region where the new group of micro-resonators was tuned for, attenuating the peaks in the vicinity. Complementing this remark, the peak at 930 Hz present in the sound power radiated for the first LRM solution is attenuated, as shown in Figure 16 that attenuating is due to the movement of the masses of the micro-

Frequency Band [Hz]	LRM1	LRM2
50-5000	85,22%	82,38%
50-1000	89,00%	98,30%
1000-5000	85,22%	82,38%

Table 1: Relative reduction in the normalized sound power radiated for LRM1 and LRM2.

resonators in the second group. The amplitude of the secondary peak after the first BG, around 500 Hz, was also decreased with the LRM2 solution.

At higher frequencies, both LRM solutions exhibit a comparable trend of attenuation. Nonetheless, it's noticeable that the solution with a single group of micro-resonators shows marginally higher attenuation in certain frequency ranges, while the solution with two groups of micro-resonators exhibits slightly higher attenuation in other frequency regions. The ratio of the sound power radiated to the power injected in the structure was again calculated according to Equation 6 for all the configurations. The ratio is depicted in Figure 17 for the original GBH, the lightweight GBH, the lightweight GBH with one group of micro-resonators LRM solution applied and the lightweight GBH with two groups of micro-resonators LRM solution applied. It is possible to observe the same trends in the normalized results as in the nominal results for the sound power radiated. In order to compare the effectiveness of both LRM solutions, Table 1 depicts the relative reduction in the normalized sound power radiated for LRM1 and LRM2, considering three different frequency bands. It can be noticed that the solution with two groups of micro-resonators provided a higher noise attenuation in the lower frequency band. On the other hand, the solution with a single group of micro-resonators showed a higher relative noise attenuation over the considered full spectrum (from 50 to 5000 Hz).

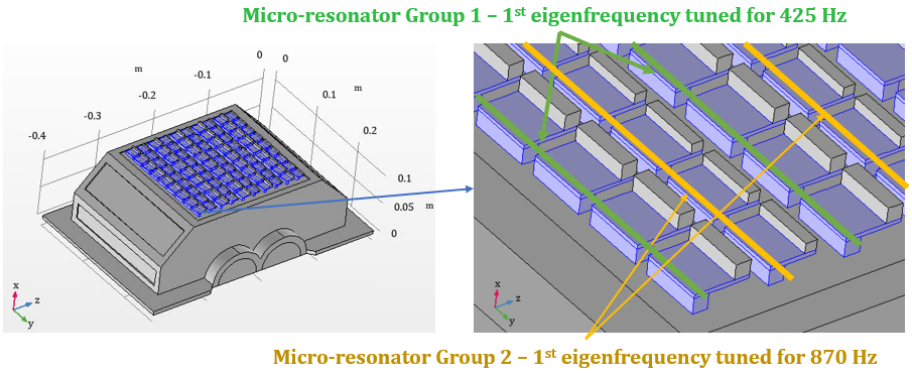

Figure 14: Lightweight GBH with LRM solution with 2 groups of micro-resonators applied in the top of the GBH (LRM2).

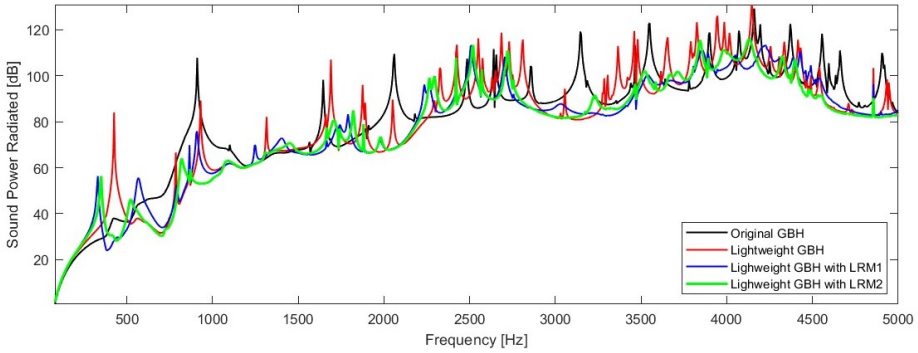

Figure 15: Sound power radiated comparison between the original GBH (black), the lightweight GBH (red), the lightweight GBH with the LRM1 solution applied (blue) and the lightweight GBH with the LRM2 solution (green).

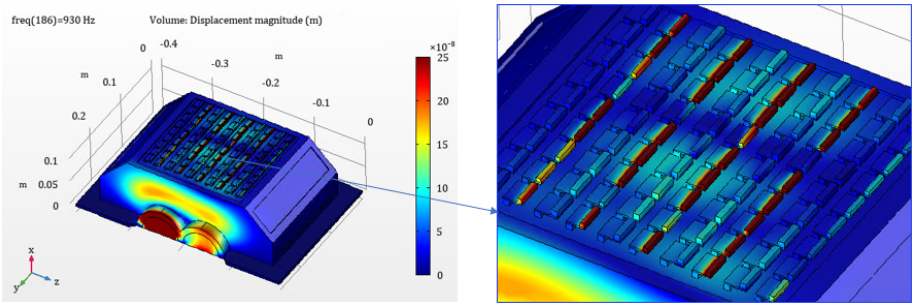

Figure 16: Displacement of the lightweight GBH with the LRM2 solution at 930 Hz.

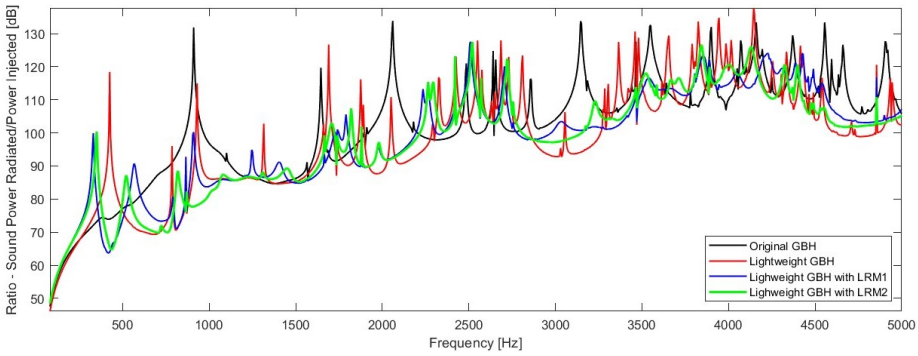

Figure 17: Ratio between the sound power radiated and the power injected in the structure of the original GBH (black), the lightweight GBH (red), the lightweight GBH with the LRM1 solution applied (blue) and the lightweight GBH with the LRM2 solution applied (green).

3.4. GBH Locally Resonant Metamaterial Solution Experimental Application

For experimental validation of the LRM solution concept, the original 2mm aluminium top plate of the manufactured housing was substituted by an LRM plate. The LRM plate consisted of an aluminium plate with 72 Acrylonitrile Butadiene Styrene (ABS)-Steel micro-resonators assembled in a rectangular pattern (20x20 mm unit cells), as seen in Figure 18. According to the process stated in the Section 3.3, the micro-resonators of the LRM solution, were tuned for the first eigenfrequency of the top plate, 393 Hz (verified experimentally). The micro-resonator width of 16 mm was maintained, the ABS base was defined as a square cross-section of 4×4 mm, the ABS beam was defined with a thickness of 1 mm and a length of 13.973 mm, and the steel mass was maintained as a square cross-section of 4×4 mm. Both the steel mass connection in each micro-resonator and the connection of each micro-resonator to the aluminum plate were made using accelerometer bonding wax.

Figure 19 shows the aluminum GBH mock-up with LRM solution applied, mounted in the test platform.

Figure 18: Close-up view of the LRM Plate (aluminium plate with 72 ABS-Steel micro-resonators) next to a 10 cent euro coin (for scale perception).

4. Experimental Results/Discussion

Figure 20 presents the average normalized normal acceleration ($m/s^2/N$) measured by the accelerometer placed in the center of the top plate, for the baseline configuration and for the LRM solution configuration. More than 30 dB vibration attenuation at the frequency where the micro-resonators were tuned. The average vibration in the center of the top plate is reduced by 40% in the full spectrum considered (50 to 5000 Hz) by the presence of the LRM solution on the housing. Table 2 summarizes the relative attenuation of vibration for all the accelerometers placed on the housing structure. The locations of each

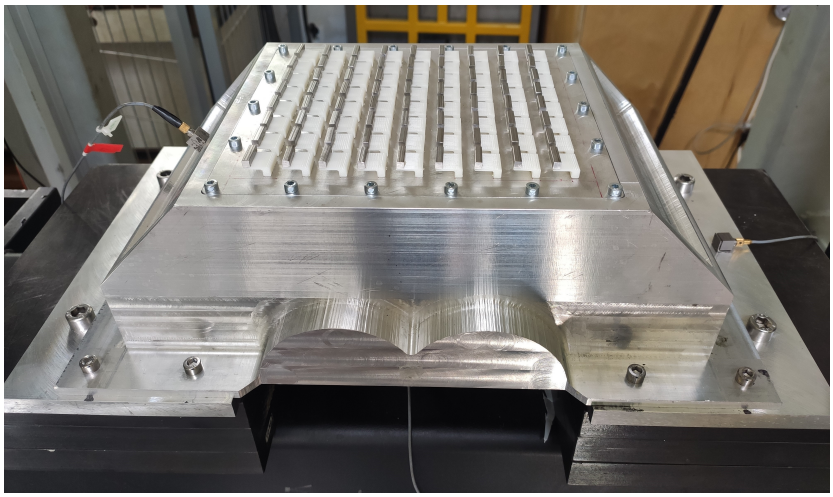

Figure 19: Aluminium GBH mock-up bolted to the experimental stand, with LRM solution applied on the top plate.

accelerometer are stated in Figure 4. The frequency responses for all the sensors are found in the appendix Appendix A.

Considering an average across the entire spectrum, it can be observed that the LRM solution yields vibration attenuation in all acceleration sensors. The most substantial reduction in acceleration occurs in the top plate, where the micro-resonators are applied (P11, P1, P2, P3, and P5). Nevertheless, some degree of acceleration attenuation is also noticeable in other regions of the GBH, where the LRM solution was not applied. For instance, at positions P9 and P7, acceleration reduction of 11% and 3%, respectively, were observed. Moreover, the acceleration results in in-plane directions in the center of the top plate (P11), show attenuation in both directions (x and y). Even though the in-plane vibration is not responsible for the noise emission, this in-plane attenuation reduces the wave propagation for other parts of the structure where those waves can be normal to the surface, hence, further attenuating the noise emission.

In order to better align with the experimental data, a new numerical model was developed in COMSOL. This model closely matches the experimental setup by adapting the geometry of the housing and setting the material to aluminum alloy. Moreover, the numerical force input was placed in the same location as the force input generated by the electrodynamic shaker in the experimental setup. The first eigenmode of the housing in the numerical model occurs at 520 Hz, whereas in the experimental setup, it is at 393 Hz. Although it would have been possible to adjust the numerical eigenfrequency to match the experimental one by modeling the full bolted connection with non-linear contacts, this was not the objective of this study. Therefore, the micro-resonators in the numerical simulation were tuned for 520 Hz to replicate the same tuning conditions as those in the experimental setup.

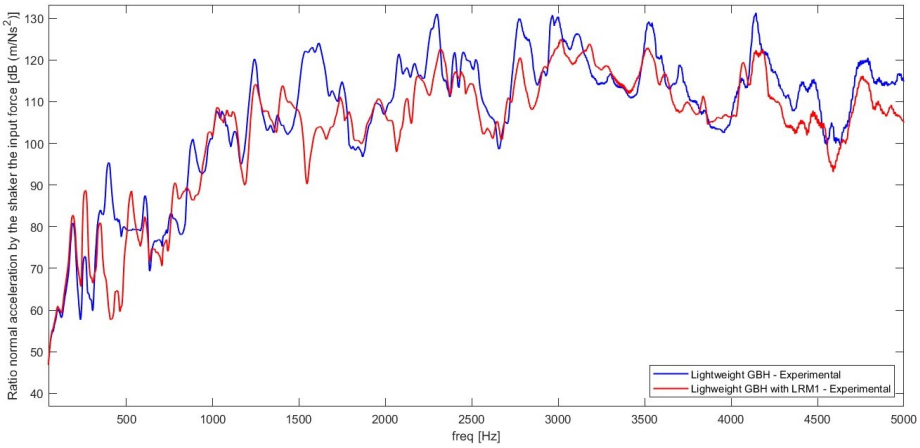

Figure 20: Normalized acceleration at the center of the top plate - Experimental.

Accelerometer Position	Baseline	LRM Applied	Relative Variation
P11z (Center)	5.757	3.457	-40%
P1	5.309	3.467	-35%
P2	5.966	3.063	-49%
P3	3.652	2.748	-25%
P5	6.528	3.981	-39%
P11x	2.508	1.806	-28%
P11y	7.190	5.027	-11%
P9	3.988	3.543	-11%
P7	4.323	4.203	-3%

Table 2: Comparison between the normalized acceleration ($m/s^2/N$) of the baseline configuration and the configuration with the LRM applied for all the accelerometers placed on the housing structure and the respective relative variation.

Figure 21 displays the normalized normal acceleration measured at the center of the top plate in the numerical simulation. Comparing the numerical and experimental results, similar trends are evident. Specifically, the micro-resonators exhibit high attenuation at the frequency they were tuned for; there is average broadband attenuation across the spectrum, and the noise/acceleration peaks shift in frequency. The numerical model assumes a fixed condition that represents higher stiffness than the actual bolted connection to the experimental stand. The boundary conditions have a considerable impact on the lower frequency range. Consequently, the vibration levels at low frequencies are lower in the numerical simulation than in the experiments. In the numerical simulation, the structure is isolated from the external environment, resulting in a clearer frequency response. Compared with the numerical results, the frequency response peaks in the experimental results are less sharp since friction contacts introduce additional damping to the system.

Table 3 displays a comparison between the experimental and numerical average results of the normalized acceleration $(m/s^2/N)$ at the center of the top plate of the baseline configuration and the configuration with the LRM applied. The absolute values of the normalized acceleration are identical for both the baseline configuration and the configuration with the LRM applied. On average, the numerical results are overestimated by 3.5% for the baseline configuration and 2.4% for the configuration with LRM applied. However, regarding the relative variation with the presence of the LRM, the value is well estimated, being the relative reduction of 40% for both experimental and numerical results.

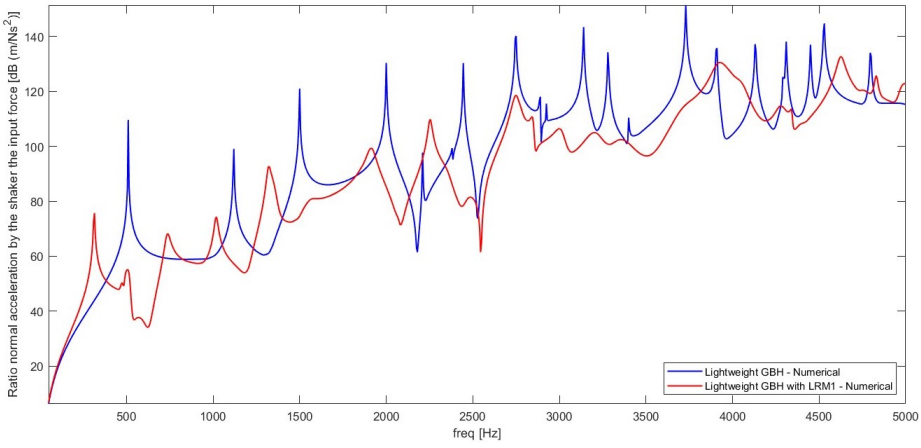

Figure 21: Normalized acceleration at the center of the top plate - Numerical.

For the purpose of discussing the impact of the acceleration attenuation on the noise emission, the sound power radiated by a vibrating structure is dependent of the square of the normal velocity of the outside surface of the structure [130]. In the frequency domain, a reduction in the acceleration amplitude implies a reduction in velocity amplitude for each frequency. Hence, disregarding

	Baseline	LRM Solution	Relative Variation
Numerical Results	5,960	3,539	-40%
Experimental Results	5,757	3,457	-40%
Error (%)	3.5%	2.4%	

Table 3: Comparison between the experimental and numerical average results of the normalized acceleration ($m/s^2/N$) at the center of the top plate of the baseline configuration and the configuration with the LRM applied, and the respective relative variation

the change in radiation efficiency, it is possible to estimate that a 40% reduction in acceleration represents a reduction of 64% in the sound power radiated by the GBH.

5. Conclusions

As initially theoretically predicted, the mass reduction of a gearbox housing degraded its noise and vibration behavior, inducing more noise emission peaks in the low-frequency range. These lower frequency noise and vibration peaks are hard to attenuate by conventional means. This work presented applications of locally resonant metamaterial solutions to attenuate the noise and vibration of a lightweight GBH.

The numerical simulation results indicate that the application of LRM solutions in GBHs can significantly reduce gearbox noise emissions. The analysis shows that the LRM solutions not only attenuate noise emission in the predicted BG but also provides a substantial average attenuation across the entire considered frequency spectrum (50-5000 Hz). In addition to the LRM solution consisting of one group of micro-resonators, a second LRM solution was analyzed, which comprised two groups of micro-resonators. This second LRM solution resulted in an even smoother response in the low-frequency range (50-1500 Hz). However, the average attenuation across the full spectrum was slightly lower compared to the LRM solution with only one group of micro-resonators.

The experimental results corroborated the LRM attenuation concept and trends observed in the numerical results, demonstrating the high attenuation on the predicted LRM BG and average broadband attenuation over the considered spectrum. The experimental results revealed that vibration was attenuated not only in the areas where the LRM solution was applied but also in other parts of the GBH where no LRM was applied. The experiments also demonstrated that in the area of the application of the LRM there was attenuation of in-plane vibration in both directions. Although in-plane vibration does not directly contribute to noise emissions, the observed attenuation in these directions can limit the propagation of waves to other parts of the GBH where they would radiate noise. This fact can further contribute to the reduction of gearbox noise emission.

The LRM solutions considered in this study results in a minimal increase in mass, typically ranging between 2% and 3% relative to the mass of the host

structure, depending on the specific design and configuration. This increase is minor compared to the 20% mass reduction achieved by transitioning from the original GBH to the lightweight GBH. Therefore, the LRM solution enables the development of a lightweight version of the GBH with improved NVH characteristics.

The proposed LRM solutions are passive, lightweight and low-cost solutions that gearbox designers can implement in GBHs to enhance their NVH characteristics. These solutions do not require a control system, only an early design study identifying the area(s) to apply the LRMs and the main frequency region to attenuate. Additionally, the LRM solutions are expected to provide broadband attenuation, which will offer additional benefits beyond the targeted frequency range.

Gearbox and EV motor manufacturers face two significant issues when introducing new ideas or design approaches: one is the added cost, and another is the short development time available to bring products to market. The objective of this work was not to optimize LRM solutions for a specific housing design, but rather to demonstrate that simple LRM solutions can effectively reduce noise emissions and vibration through the mechanisms described.

The micro-resonator spring parts were made of ABS and acrylate polymer materials in this investigation. However, it is important to note that in industrial applications for GBHs, high-temperature polyamides can be used for micro-resonator manufacturing to withstand the elevated temperatures experienced on the exterior of the GBH. To streamline the manufacturing process, researchers propose a future development where coating layers with embedded micro-resonators are bonded to housing surfaces instead of bonding each resonator individually. This approach has the potential to significantly reduce production time and costs.

The findings of this study offer a step towards the industrial application of LRMs in GBHs and EV motor housings, offering a promising solution to the current conflicting design challenges.

Acknowledgement

This project has received funding from the European Union's Horizon 2020 research and innovation programme under Marie-Curie grant agreement No 860243.

Appendices

Appendix A. Comparison between the normalized acceleration ($m/s^2/N$) of the baseline configuration and the configuration with the LRM applied for all the accelerometers placed on the housing structure

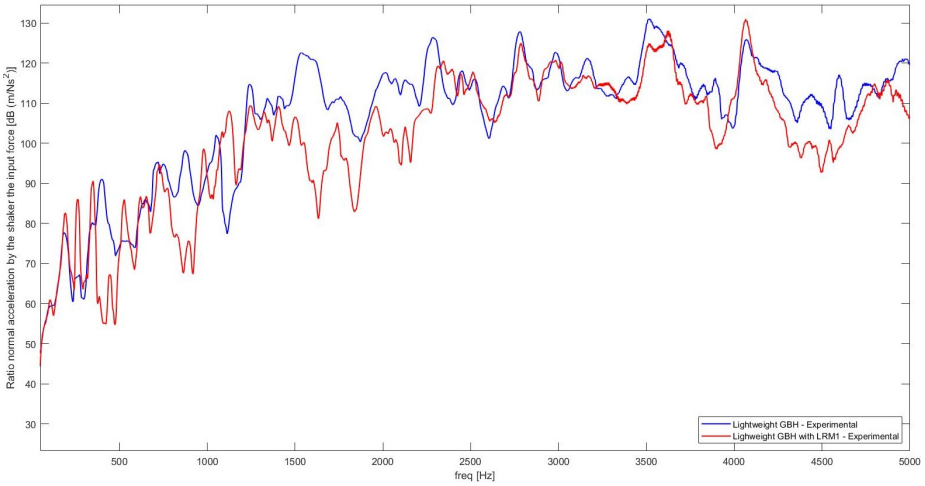

Figure Appendix A.1: Normalized acceleration at the position P1.

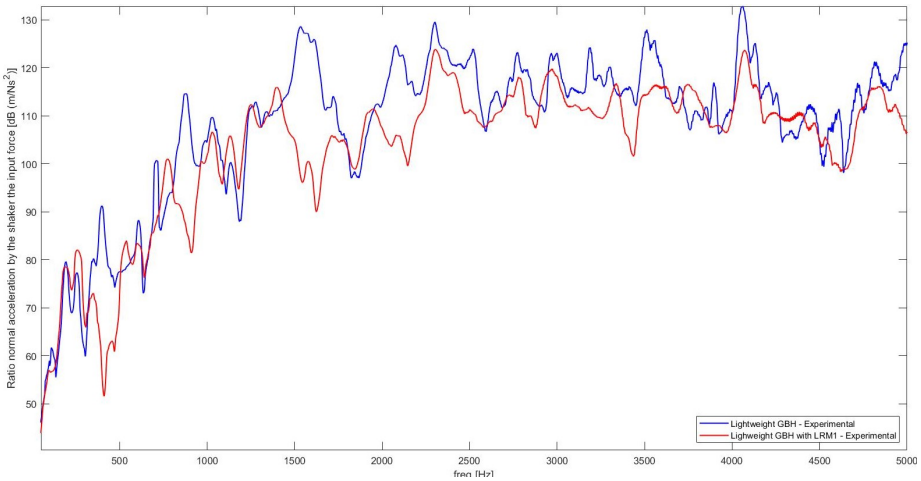

Figure Appendix A.2: Normalized acceleration at the position P2.

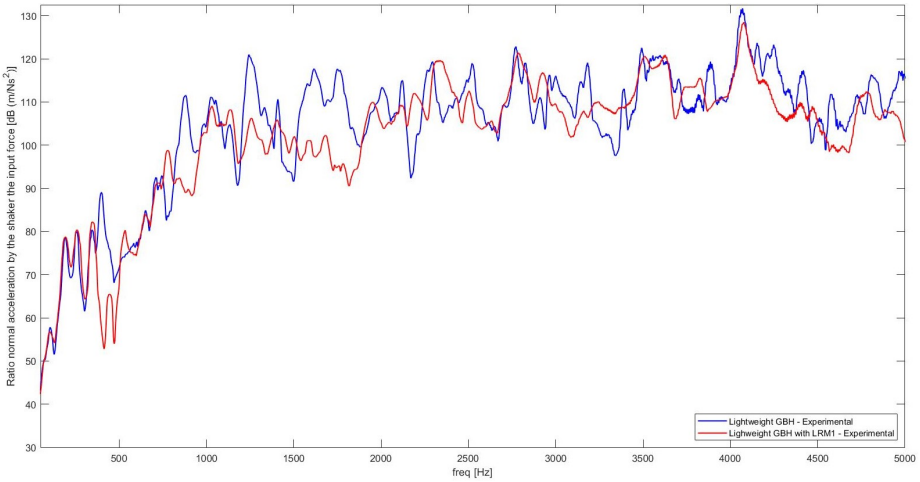

Figure Appendix A.3: Normalized acceleration at the position P3.

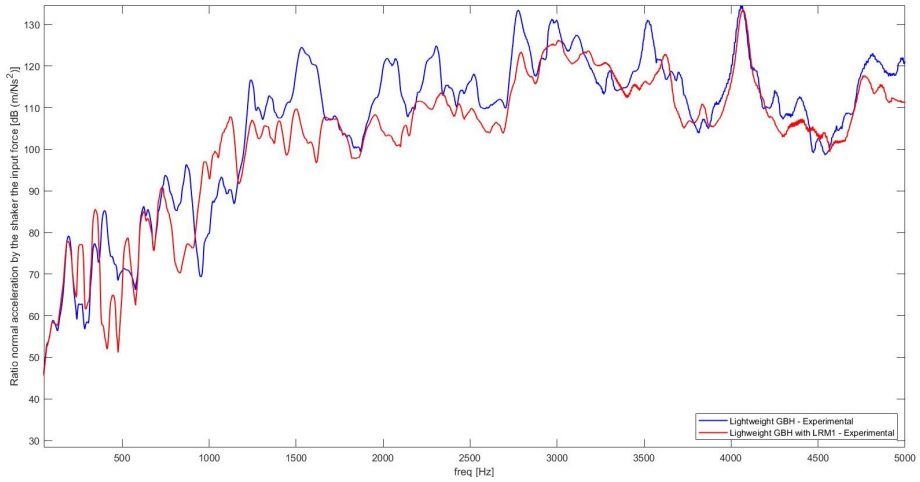

Figure Appendix A.4: Normalized acceleration at the position P5.

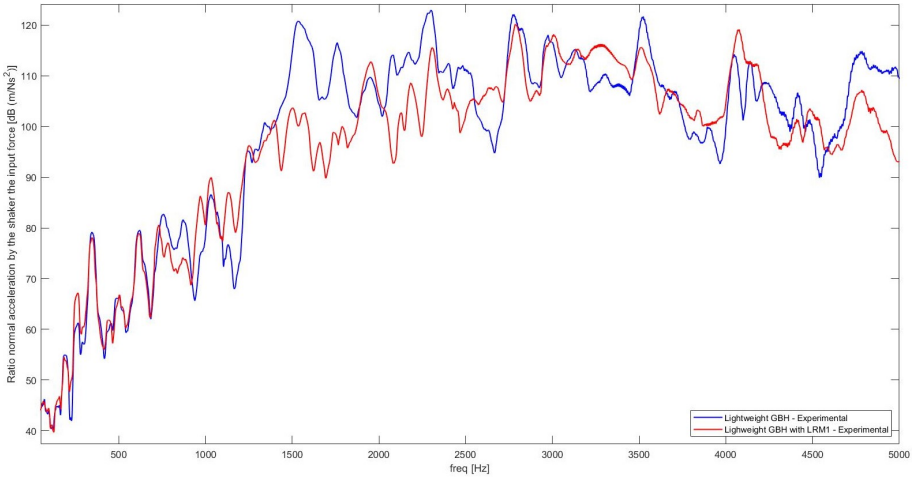

Figure Appendix A.5: Normalized acceleration at the position P11 in x direction.

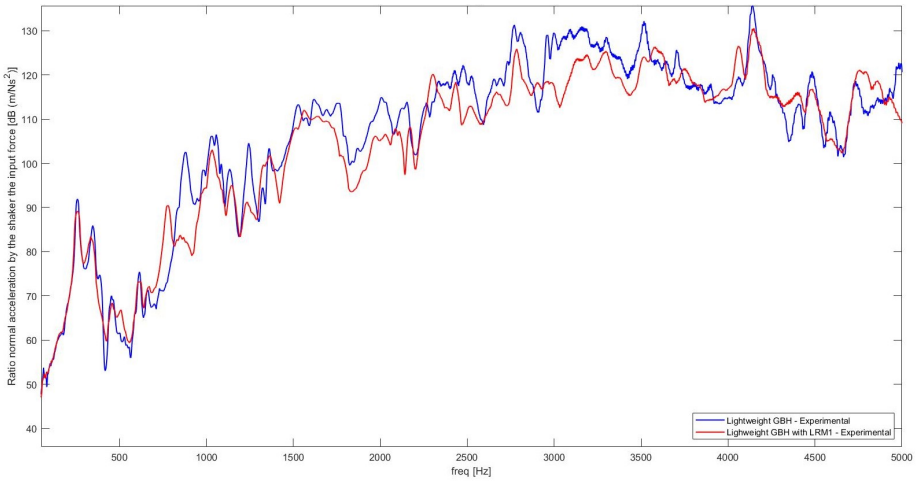

Figure Appendix A.6: Normalized acceleration at the position P11 in y direction.

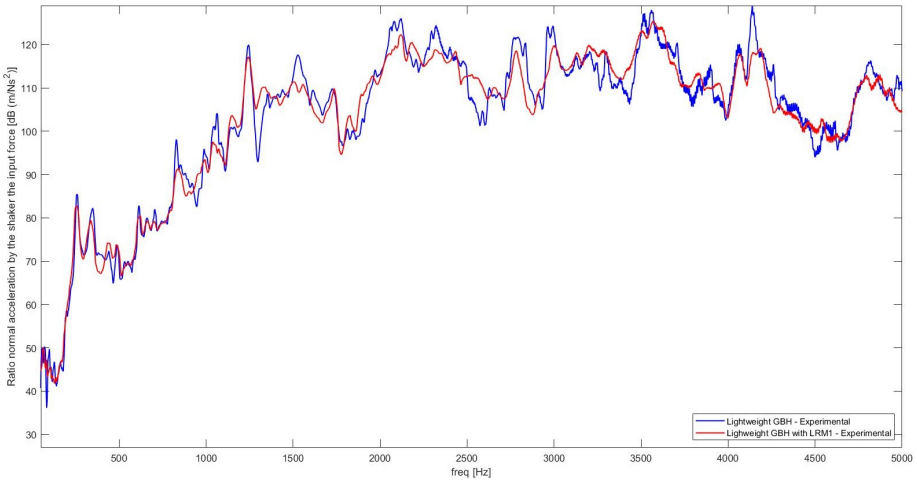

Figure Appendix A.7: Normalized acceleration at the position P9.

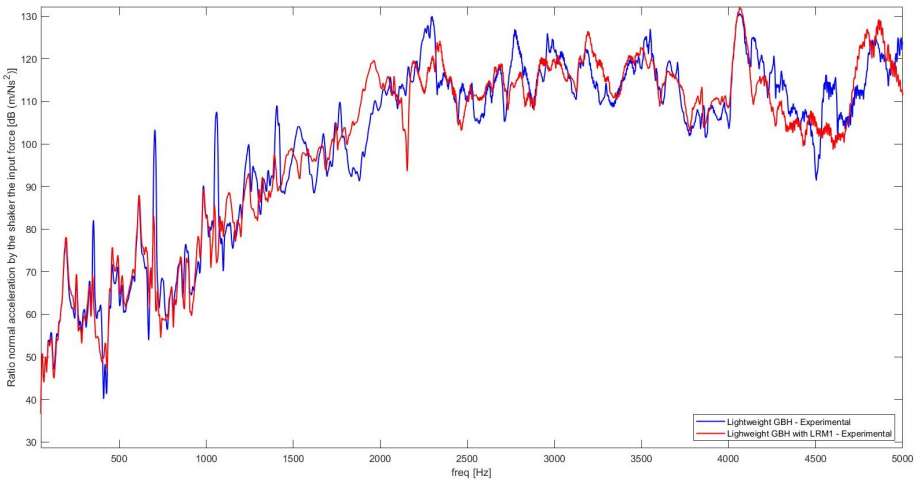

Figure Appendix A.8: Normalized acceleration at the position P7.

Appendix B. Technical drawing of the manufactured aluminium housing

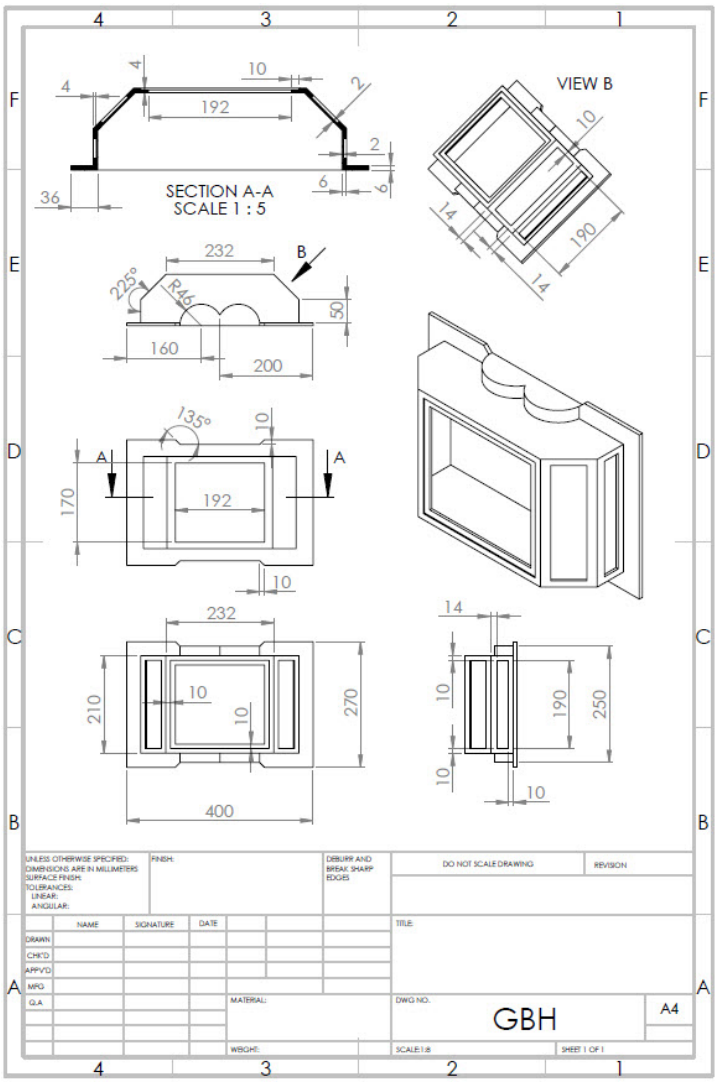

Figure Appendix B.9: Technical drawing of the manufactured aluminium housing.

References

[1] S. Slavov, M. Konsulova-Bakalova, Optimizing weight of housing elements of two-stage reducer by using the topology management optimization

capabilities integrated in SOLIDWORKS: A case study, Machines 7, doi:10.3390/machines7010009.

[2] D. Ivanov, Gearbox Housing Design – Topology Optimization through Generative Design, Ph.D. thesis (2018).

[3] L. Ling, Y. Huang, Topology optimization design of gearbox housing in electric bus, Applied Mechanics and Materials 574, doi:10.4028/www.scientific.net/AMM.574.173.

[4] G. Maidanik, Response of ribbed panels to reverberant acoustic fields, The journal of the Acoustical Society of America 34, doi:10.1121/1.1918200.

[5] A. Berry, J. Nicolas, Structural acoustics and vibration behavior of complex panels, Applied Acoustics 43 (3), doi:10.1016/0003-682X(94)90047-7.

[6] F. J. Fahy, P. Gardonio, Sound and Structural Vibration: Radiation, Transmission and Response, EngineeringPro collection, Elsevier Science, 2007.

[7] J. U. Surjadi, L. Gao, H. Du, X. Li, X. Xiong, N. X. Fang, Y. Lu, Mechanical Metamaterials and Their Engineering Applications, Advanced Engineering Materials 21 (3), doi:10.1002/adem.201800864.

[8] D. Del Vescovo, I. Giorgio, Dynamic problems for metamaterials: Review of existing models and ideas for further research, International Journal of Engineering Science 80, doi:10.1016/j.ijengsci.2014.02.022.

[9] G. Ma, P. Sheng, Acoustic metamaterials: From local resonances to broad horizons, Science Advances 2 (2), doi:10.1126/sciadv.1501595.

[10] N. F. Melo, C. Claeys, E. Deckers, B. Pluymers, W. Desmet, Dynamic Metamaterials for Structural Stopband Creation, SAE International Journal of Passenger Cars - Mechanical Systems 9 (3), doi:10.4271/2016-01-1791.

[11] C. Claeys, N. G. Rocha de Melo Filho, L. Van Belle, E. Deckers, W. Desmet, Design and validation of metamaterials for multiple structural stop bands in waveguides, Extreme Mechanics Letters 12, doi:10.1016/j.eml.2016.08.005.

[12] A. Banerjee, R. Das, E. P. Calius, Waves in Structured Mediums or Metamaterials: A Review, Archives of Computational Methods in Engineering 26 (4), doi:10.1007/s11831-018-9268-1.

[13] P. Deymier, Acoustic Metamaterials and Phononic Crystals (Springer Series in Solid-State Sciences), Springer-Verlag Berlin Heidelberg, 2013.

[14] D. Schurig, J. Mock, B. J. Justice, S. Cummer, J. Pendry, A. Starr, D. Smith, Metamaterial Electromagnetic Cloak at Microwave Frequencies, Science 314, doi:10.1126/science.1133628.

[15] J. Christensen, M. Kadic, O. Kraft, M. Wegener, Vibrant times for mechanical metamaterials, MRS Communications 5 (3), doi:10.1557/mrc.2015.51.

[16] M. H. Lu, L. Feng, Y. F. Chen, Phononic crystals and acoustic metamaterials, Materials Today 12 (12), doi:10.1016/S1369-7021(09)70315-3.

[17] V. M. Shalaev, Physics: Transforming light, Science 322 (5900), doi:10.1126/science.1166079.

[18] E. Barchiesi, M. Spagnuolo, L. Placidi, Mechanical metamaterials: a state of the art, Mathematics and Mechanics of Solids 24 (1), doi:10.1177/1081286517735695.

[19] A. A. Zadpoor, Mechanical meta-materials, Materials Horizons 3 (5), doi:10.1039/c6mh00065g.

[20] K. Bertoldi, V. Vitelli, J. Christensen, M. Van Hecke, Flexible mechanical metamaterials, Nature Reviews Materials 2, doi:10.1038/natrevmats.2017.66.

[21] D. Attard, J. N. Grima, A three-dimensional rotating rigid units network exhibiting negative Poisson's ratios, Physica Status Solidi (B) Basic Research 249 (7), doi:10.1002/pssb.201084223.

[22] G. Acar, C. Yilmaz, Experimental and numerical evidence for the existence of wide and deep phononic gaps induced by inertial amplification in two-dimensional solid structures, Journal of Sound and Vibration 332 (24), doi:10.1016/j.jsv.2013.06.022.

[23] S. Krödel, N. Thomé, C. Daraio, Wide band-gap seismic metastructures, Extreme Mechanics Letters 4, doi:10.1016/j.eml.2015.05.004.

[24] M. Brun, S. Guenneau, A. B. Movchan, Achieving control of in-plane elastic waves, Applied Physics Letters 94 (6), doi:10.1063/1.3068491.

[25] A. H. Wilson, The theory of electronic semi-conductors, Proceedings of the Royal Society of London. Series A, Containing Papers of a Mathematical and Physical Character 133 (822), doi:10.1098/rspa.1931.0162.

[26] L. Solymar, D. Walsh, R. R. A. Syms, The band theory of solids, in: Electrical Properties of Materials, Oxford University Press, 2018, doi:10.1093/oso/9780198829942.003.0007.

[27] E. Yablonovitch, Inhibited spontaneous emission in solid-state physics and electronics, Physical review letters 58 (20), doi:10.1103/PhysRevLett.58.2059.

[28] K. M. Ho, C. T. Chan, C. M. Soukoulis, Existence of a photonic gap in periodic dielectric structures, Physical Review Letters 65 (25), doi:10.1103/PhysRevLett.65.3152.

[29] E. Yablonovitch, T. J. Gmitter, K.-M. Leung, Photonic band structure: The face-centered-cubic case employing nonspherical atoms, Physical review letters 67 (17), doi:10.1103/PhysRevLett.67.2295.

[30] M. M. Sigalas, E. N. Economou, Elastic and Acoustic Wave Band Structure, Physics 158, doi:10.1016/0022-460X(92)90059-7.

[31] M. S. Kushwaha, P. Halevi, L. Dobrzynski, B. Djafari-Rouhani, Acoustic band structure of periodic elastic composites, Physical Review Letters 71 (13), doi:10.1103/PhysRevLett.71.2022.

[32] S. M. Girvin, K. Yang, Modern condensed matter physics, Cambridge University Press, 2019, doi:10.1017/9781316480649.

[33] R. Martínez-Sala, J. Sancho, J. V. Sánchez, V. Gómez, J. Llinares, F. Meseguer, Sound attenuation by sculpture, Nature 378 (6554), doi:10.1038/378241a0.

[34] M. S. Kushwaha, Stop-bands for periodic metallic rods : Sculptures that can filter the noise, Applied Physics Letters, doi:10.1063/1.119130.

[35] C. Goffaux, F. Maseri, J. O. Vasseur, B. Djafari-Rouhani, P. Lambin, Measurements and calculations of the sound attenuation by a phononic band gap structure suitable for an insulating partition application, Applied Physics Letters 83 (2), doi:10.1063/1.1592016.

[36] J. V. Sánchez-Pérez, D. Caballero, R. Mártinez-Sala, C. Rubio, J. Sánchez-Dehesa, F. Meseguer, J. Llinares, F. Gálvez, Sound attenuation by a two-dimensional array of rigid cylinders, Physical Review Letters 80 (24), doi:10.1103/PhysRevLett.80.5325.

[37] D. Caballero, J. Sánchez-Dehesa, C. Rubio, R. Mártinez-Sala, J. V. Sánchez-Pérez, F. Meseguer, J. Llinares, Large two-dimensional sonic band gaps, Physical Review E - Statistical Physics, Plasmas, Fluids, and Related Interdisciplinary Topics 60 (6), doi:10.1103/PhysRevE.60.R6316.

[38] J. O. Vasseur, P. A. Deymier, G. Frantziskonis, G. Hong, B. Djafari-Rouhani, L. Dobrzynski, Experimental evidence for the existence of absolute acoustic band gaps in two-dimensional periodic composite media, Journal of Physics Condensed Matter 10 (27), doi:10.1088/0953-8984/10/27/006.

[39] M. Maldovan, E. L. Thomas, Periodic Materials and Interference Lithography for Photonics, Phononics and Mechanics, 2009.

[40] D. Bria, B. Djafari-Rouhani, A. Bousfia, E. B. El Houssaine, A. Nougaoui, Absolute acoustic band gap in coupled multilayer structures, EPL (Europhysics Letters) 55, doi:10.1209/epl/i2001-00357-4.

[41] D. Bria, B. Djafari-Rouhani, Omnidirectional elastic band gap in finite lamellar structures, Physical review E, Statistical, nonlinear, and soft matter physics 66, doi:10.1103/PhysRevE.66.056609.

[42] B. Manzanares-Martínez, J. Sánchez-Dehesa, A. Håkansson, F. Cervera, F. Ramos-Mendieta, Experimental evidence of omnidirectional elastic bandgap in finite one-dimensional phononic systems, Applied Physics Letters 85 (1), doi:10.1063/1.1766074.

[43] P. Langlet, A.-C. Hladky-Hennion, J.-N. Decarpigny, Analysis of the propagation of plane acoustic waves in passive periodic materials using the finite element method, Journal of The Acoustical Society of America 98 (4), doi:10.1121/1.413244.

[44] I. E. Psarobas, A. Modinos, R. Sainidou, N. Stefanou, Acoustic properties of colloidal crystals, Physical Review B - Condensed Matter and Materials Physics 65 (6), doi:10.1103/PhysRevB.65.064307.

[45] T. Delpero, S. Schoenwald, A. Zemp, A. Bergamini, Structural engineering of three-dimensional phononic crystals, Journal of Sound and Vibration 363, doi:10.1016/j.jsv.2015.10.033.

[46] T. Delpero, G. Hannema, B. Van Damme, S. Schoenwald, A. Zemp, A. Bergamini, Inertia amplification in phononic crystals for low frequency bandgaps, 8th Conference on Smart Structures and Materials, SMART 2017 and 6th International Conference on Smart Materials and Nanotechnology in Engineering, SMN 2017 (June).

[47] B. Van Damme, G. Hannema, A. Zemp, Sound transmission through checkerboard sandwich panels, ISMA conference on Noise and Vibration Engineering.

[48] J. N. Kirchhof, K. Weinel, S. Heeg, V. Deinhart, S. Kovalchuk, K. Höflich, K. I. Bolotin, Tunable Graphene Phononic Crystal, Nano Letters, doi:10.1021/acs.nanolett.0c04986.

[49] C. Goffaux, J. Sánchez-Dehesa, A. L. Yeyati, P. Lambin, A. Khelif, J. O. Vasseur, B. Djafari-Rouhani, Evidence of Fano-like interference phenomena in locally resonant materials, Physical Review Letters 88 (22), doi:10.1103/PhysRevLett.88.225502.

[50] L. Fredianelli, A. Del Pizzo, G. Licitra, Recent developments in sonic crystals as barriers for road traffic noise mitigation, Environments - MDPI 6 (2), doi:10.3390/environments6020014.

[51] L. Chalmers, D. P. Elford, F. V. Kusmartsev, G. M. Swallowe, Acoustic band gap formation in two-dimensional locally resonant sonic crystals comprised of helmholtz resonators, International Journal of Modern Physics B 23 (20-21), doi:10.1142/s0217979209063390.

[52] D. P. Elford, L. Chalmers, F. V. Kusmartsev, G. M. Swallowe, Matryoshka locally resonant sonic crystal, The Journal of the Acoustical Society of America 130 (5), arXiv:1102.0399, doi:10.1121/1.3643818.

[53] Z. Liu, X. Zhang, Y. Mao, Y. Y. Zhu, Z. Yang, C. T. Chan, P. Sheng, Locally resonant sonic materials, Science 289 (5485), doi:10.1126/science.289.5485.1734.

[54] P. Sheng, X. X. Zhang, Z. Liu, C. T. Chan, Locally resonant sonic materials, Physica B: Condensed Matter 338 (1-4), doi:10.1016/S0921-4526(03)00487-3.

[55] F. Langfeldt, W. Gleine, Membrane- and plate-type acoustic metamaterials with elastic unit cell edges, Journal of Sound and Vibration 453, doi:10.1016/j.jsv.2019.04.018.

[56] J. Park, D. Lee, J. Rho, Recent advances in non-traditional elastic wave manipulation by macroscopic artificial structures, Applied Sciences (Switzerland) 10 (2), doi:10.3390/app10020547.

[57] J. H. Oh, H. Min Seung, Y. Young Kim, A truly hyperbolic elastic metamaterial lens, Applied Physics Letters 104 (7), doi:10.1063/1.4865907.

[58] M. Oudich, M. Senesi, M. B. Assouar, M. Ruzenne, J. H. Sun, B. Vincent, Z. Hou, T. T. Wu, Experimental evidence of locally resonant sonic band gap in two-dimensional phononic stubbed plates, Physical Review B - Condensed Matter and Materials Physics 84 (16), doi:10.1103/PhysRevB.84.165136.

[59] V. G. Veselago, The Electrodynamic of Substances with Simultaneous Negative Values of E and μ, Soviet Physics Uspekhi 10 (4), doi:10.1070/PU1968v010n04ABEH003699.

[60] J. B. Pendry, A. J. Holden, D. J. Robbins, W. J. Stewart, Magnetism from conductors and enhanced nonlinear phenomena, IEEE Transactions on Microwave Theory and Techniques 47 (11), doi:10.1109/22.798002.

[61] P. Sheng, J. Mei, Z. Liu, W. Wen, Dynamic mass density and acoustic metamaterials, Physica B: Condensed Matter 394 (2), doi:10.1016/j.physb.2006.12.046.

[62] A. O. Krushynska, V. G. Kouznetsova, M. G. D. Geers, Towards optimal design of locally resonant acoustic metamaterials, Journal of the Mechanics and Physics of Solids 71 (1), doi:10.1016/j.jmps.2014.07.004.

[63] Z. Liu, C. T. Chan, P. Sheng, Analytic model of phononic crystals with local resonances, Physical Review B - Condensed Matter and Materials Physics 71 (1), doi:10.1103/PhysRevB.71.014103.

[64] J. Li, C. T. Chan, Double-negative acoustic metamaterial, Physical Review E - Statistical Physics, Plasmas, Fluids, and Related Interdisciplinary Topics 70 (5), doi:10.1103/PhysRevE.70.055602.

[65] E. P. Calius, X. Bremaud, B. Smith, A. Hall, Negative mass sound shielding structures: Early results, Physica Status Solidi (B) Basic Research 246 (9), doi:10.1002/pssb.200982040.

[66] E. C. Wester, X. Brémaud, B. Smith, Meta-Material Sound Insulation 16 (1), doi:10.1260/135101009788066555.

[67] W. Xiao, G. W. Zeng, Y. S. Cheng, Flexural vibration band gaps in a thin plate containing a periodic array of hemmed discs, Applied Acoustics 69 (3), doi:10.1016/j.apacoust.2006.09.003.

[68] C. Comi, L. Driemeier, Wave propagation in cellular locally resonant metamaterials, Latin American Journal of Solids and Structures 15 (4), doi:10.1590/1679-78254327.

[69] X. Hu, C. T. Chan, J. Zi, Two-dimensional sonic crystals with Helmholtz resonators, Physical Review E - Statistical, Nonlinear, and Soft Matter Physics 71 (5), doi:10.1103/PhysRevE.71.055601.

[70] G. Wang, X. Wen, J. Wen, Y. Liu, Quasi-one-dimensional periodic structure with locally resonant band gap, Journal of Applied Mechanics, Transactions ASME 73 (1), doi:10.1115/1.2061947.

[71] L. Liu, M. I. Hussein, Wave motion in periodic flexural beams and characterization of the transition between bragg scattering and local resonance, Journal of Applied Mechanics, Transactions ASME 79 (1), doi:10.1115/1.4004592.

[72] Y. Xiao, J. Wen, D. Yu, X. Wen, Flexural wave propagation in beams with periodically attached vibration absorbers: Band-gap behavior and band formation mechanisms, Journal of Sound and Vibration 332 (4), doi:10.1016/j.jsv.2012.09.035.

[73] Y. Xiao, J. Wen, G. Wang, X. Wen, Theoretical and experimental study of locally resonant and bragg band gaps in flexural beams carrying periodic arrays of beam-like resonators, Journal of Vibration and Acoustics, Transactions of the ASME 135 (4), doi:10.1115/1.4024214.

[74] C. C. Claeys, K. Vergote, P. Sas, W. Desmet, On the potential of tuned resonators to obtain low-frequency vibrational stop bands in periodic panels, Journal of Sound and Vibration 332 (6), doi:10.1016/j.jsv.2012.09.047.

[75] T. T. Wu, Z. G. Huang, T. C. Tsai, T. C. Wu, Evidence of complete band gap and resonances in a plate with periodic stubbed surface, Applied Physics Letters 93 (11), doi:10.1063/1.2970992.

[76] M. Badreddine Assouar, M. Senesi, M. Oudich, M. Ruzzene, Z. Hou, Broadband plate-type acoustic metamaterial for low-frequency sound attenuation, Applied Physics Letters 101 (17), doi:10.1063/1.4764072.

[77] Y. Xiao, J. Wen, X. Wen, Flexural wave band gaps in locally resonant thin plates with periodically attached springmass resonators, Journal of Physics D: Applied Physics 45 (19), doi:10.1088/0022-3727/45/19/195401.

[78] C. C. Claeys, P. Sas, W. Desmet, On the acoustic radiation efficiency of local resonance based stop band materials, Journal of Sound and Vibration 333 (14), doi:10.1016/j.jsv.2014.03.019.

[79] Y. Xiao, J. Wen, L. Huang, X. Wen, Analysis and experimental realization of locally resonant phononic plates carrying a periodic array of beam-like resonators, Journal of Physics D: Applied Physics 47 (4), doi:10.1088/0022-3727/47/4/045307.

[80] A. Hall, E. P. Calius, G. Dodd, K. L. Chan, Development of locally resonant structures for sonic barriers, Health Monitoring of Structural and Biological Systems 2013 8695, doi:10.1117/12.2024999.

[81] P. Li, S. Yao, X. Zhou, G. Huang, G. Hu, Effective medium theory of thin-plate acoustic metamaterials, The Journal of the Acoustical Society of America 135 (4), doi:10.1121/1.4868400.

[82] J. Li, S. Li, Sound transmission through metamaterial-based double-panel structures with poroelastic cores, Acta Acustica united with Acustica 103 (5), doi:10.3813/AAA.919114.

[83] C. Li, Optimum multiple tuned mass dampers for structures under the ground acceleration based on DDMF and ADMF, Earthquake Engineering and Structural Dynamics 31 (4), doi:10.1002/eqe.128.

[84] E. Bachy, K. Jaboviste, E. Sadoulet-Reboul, N. Peyret, G. Chevallier, C. Arnould, E. Collard, Investigations on the performance and the robustness of a metabsorber designed for structural vibration mitigation, Mechanical Systems and Signal Processing 170 (May), doi:10.1016/j.ymssp.2022.108830.

[85] Z. Yang, J. Mei, M. Yang, N. H. Chan, P. Sheng, Membrane-type acoustic metamaterial with negative dynamic mass, Physical Review Letters 101 (20), doi:10.1103/PhysRevLett.101.204301.

[86] Z. Yang, H. M. Dai, N. H. Chan, G. C. Ma, P. Sheng, Acoustic metamaterial panels for sound attenuation in the 50-1000 Hz regime, Applied Physics Letters 96 (4), doi:10.1063/1.3299007.

[87] S. Kumar, P. Bhushan, O. Prakash, S. Bhattacharya, Double negative acoustic metastructure for attenuation of acoustic emissions, Applied Physics Letters 112 (10), doi:10.1063/1.5022602.

[88] Y. Li, Y. Zhang, S. Xie, A lightweight multilayer honeycomb membrane-type acoustic metamaterial, Applied Acoustics 168, doi:10.1016/j.apacoust.2020.107427.

[89] Y. Zhang, J. Wen, Y. Xiao, X. Wen, J. Wang, Theoretical investigation of the sound attenuation of membrane-type acoustic metamaterials, Physics Letters, Section A: General, Atomic and Solid State Physics 376 (17), doi:10.1016/j.physleta.2012.03.010.

[90] F. Langfeldt, W. Gleine, O. Von Estorff, Analytical model for low-frequency transmission loss calculation of membranes loaded with arbitrarily shaped masses, Journal of Sound and Vibration 349, doi:10.1016/j.jsv.2015.03.037.

[91] F. Langfeldt, W. Gleine, O. von Estorff, An efficient analytical model for baffled, multi-celled membrane-type acoustic metamaterial panels, Journal of Sound and Vibration 417, doi:10.1016/j.jsv.2017.12.018.

[92] A. O. Krushynska, M. Miniaci, V. G. Kouznetsova, M. G. D. Geers, Multilayered inclusions in locally resonant metamaterials: Two-dimensional versus three-dimensional modeling, Journal of Vibration and Acoustics, Transactions of the ASME 139 (2), doi:10.1115/1.4035307.

[93] L. Van Belle, C. Claeys, E. Deckers, W. Desmet, The acoustic insulation performance of infinite and finite locally resonant metamaterial and phononic crystal plates, MATEC Web of Conferences 283 (June), doi:10.1051/matecconf/201928309003.

[94] C. Claeys, E. Deckers, B. Pluymers, W. Desmet, A lightweight vibro-acoustic metamaterial demonstrator: Numerical and experimental investigation, Mechanical Systems and Signal Processing 70-71, doi:10.1016/j.ymssp.2015.08.029.

[95] L. Sangiuliano, C. Claeys, E. Deckers, B. Pluymers, W. Desmet, Force Isolation by Locally Resonant Metamaterials to Reduce NVH, SAE Technical Papers 2018 (June), doi:10.4271/2018-01-1544.

[96] J. Yu, C. Nerse, G. Lee, S. Wang, C. Kyoung-Jin, Mass production applicable locally resonant metamaterials for NVH applications, in: Proceedings of the 26th International Congress on Sound and Vibration, ICSV26, Montreal, 2019.

[97] J. Jung, H. G. Kim, S. Goo, K. J. Chang, S. Wang, Realisation of a locally resonant metamaterial on the automobile panel structure to reduce noise radiation, Mechanical Systems and Signal Processing 122, doi:10.1016/j.ymssp.2018.11.050.

[98] C. Droz, O. Robin, M. Ichchou, N. Atalla, Improving sound transmission loss at ring frequency of a curved panel using tunable 3D-printed small-scale resonators, The Journal of the Acoustical Society of America 145 (1), doi:10.1121/1.5088036.

[99] K. J. Chang, N. G. Rocha de Melo Filho, L. Van Belle, C. Claeys, W. Desmet, A study on the application of locally resonant acoustic metamaterial for reducing a vehicle's engine noise, Inter-Noise 2019 - 48th International Congress and Exhibition on Noise Control Engineering.

[100] L. Sangiuliano, C. Claeys, E. Deckers, J. De Smet, B. Pluymers, W. Desmet, Reducing Vehicle Interior NVH by Means of Locally Resonant Metamaterial Patches on Rear Shock Towers, SAE Technical Papers 2019 (June), doi:10.4271/2019-01-1502.

[101] X. W. Yang, J. S. Lee, Y. Y. Kim, Effective mass density based topology optimization of locally resonant acoustic metamaterials for bandgap maximization, Journal of Sound and Vibration 383, doi:10.1016/j.jsv.2016.07.022.

[102] Y. Chen, X. Huang, G. Sun, X. Yan, G. Li, Maximizing spatial decay of evanescent waves in phononic crystals by topology optimization, Computers and Structures 182, doi:10.1016/j.compstruc.2017.01.001.

[103] J. Kook, J. S. Jensen, Topology optimization of periodic microstructures for enhanced loss factor using acoustic–structure interaction, International Journal of Solids and Structures 122-123, doi:10.1016/j.ijsolstr.2017.06.001.

[104] M. Wormser, F. Wein, M. Stingl, C. Körner, Design and additive manufacturing of 3D phononic band gap structures based on gradient based optimization, Materials 10 (10), doi:10.3390/ma10101125.

[105] X. K. Han, Z. Zhang, Topological Optimization of Phononic Crystal Thin Plate by a Genetic Algorithm, Scientific Reports 9 (1), doi:10.1038/s41598-019-44850-8.

[106] L. van Belle, N. G. de Melo Filho, M. C. Villanueva, C. Claeys, E. Deckers, F. Naets, W. Desmet, Fast metamaterial design optimization using reduced order unit cell modeling, in: Proceedings of ISMA 2020 - International Conference on Noise and Vibration Engineering and USD 2020 - International Conference on Uncertainty in Structural Dynamics, 2020, pp. 2487–2501.

[107] F. A. Pires, C. Claeys, E. Deckers, W. Desmet, The impact of resonant additions' footprint on the stop band behavior of 1D locally resonant metamaterial realizations, Journal of Sound and Vibration 491, doi:10.1016/j.jsv.2020.115705.

[108] S. Elias, V. Matsagar, Research developments in vibration control of structures using passive tuned mass dampers, Annual Reviews in Control 44, doi:10.1016/j.arcontrol.2017.09.015.

[109] J. G. Kim, G. A. Gang, S. J. Cho, G. H. Lee, Y. J. Park, Dynamic stiffness effect of mechanical components on gear mesh misalignment, Applied Sciences (Switzerland) 8 (6), doi:10.3390/app8060844.

[110] L. S. Vellar, S. P. Ontiveros-Pérez, L. F. F. Miguel, L. F. Fadel Miguel, Robust Optimum Design of Multiple Tuned Mass Dampers for Vibration Control in Buildings Subjected to Seismic Excitation, Shock and Vibration 2019, doi:10.1155/2019/9273714.

[111] M. M. Americano da Costa, D. A. Castello, C. Magluta, N. Roitman, On the optimal design and robustness of spatially distributed tuned mass dampers, Mechanical Systems and Signal Processing 150, doi:10.1016/j.ymssp.2020.107289.

[112] S. Zouari, J. Brocail, J. M. Génevaux, Flexural wave band gaps in metamaterial plates: A numerical and experimental study from infinite to finite models, Journal of Sound and Vibration 435, doi:10.1016/j.jsv.2018.07.030.

[113] D. Beli, A. T. Fabro, M. Ruzzene, J. R. F. Arruda, Wave attenuation and trapping in 3D printed cantilever-in-mass metamaterials with spatially correlated variability, Scientific Reports 9 (1), doi:10.1038/s41598-019-41999-0.

[114] A. T. Fabro, H. Meng, D. Chronopoulos, Uncertainties in the attenuation performance of a multi-frequency metastructure from additive manufacturing, Mechanical Systems and Signal Processing 138, doi:10.1016/j.ymssp.2019.106557.

[115] T. Figlus, M. Kozioł, Ł. Kuczyński, The effect of selected operational factors on the vibroactivity of upper gearbox housings made of composite materials, Sensors (Switzerland), doi:10.3390/s19194240.

[116] T. Figlus, M. Kozioł, Ł. Kuczyński, Impact of application of selected composite materials on the weight and vibroactivity of the upper gearbox housing, Materials 12 (16), doi:10.3390/ma12162517.

[117] J.-P. Berenger, A perfectly matched layer for the absorption of electromagnetic waves, Journal of Computational Physics 114 (2), doi:10.1006/jcph.1994.1159.

[118] T. Weisser, E. Foltête, N. Bouhaddi, L. O. Gonidou, A power flow mode approach dedicated to structural interface dynamic characterization, Journal of Sound and Vibration 334, doi:10.1016/j.jsv.2014.09.012.

[119] C. R. Fuller, R. L. Harne, Advanced passive treatment of low frequency sound and vibration, Annual Conference of the Australian Acoustical Society 2009 - Acoustics 2009: Research to Consulting (November).

[120] L. Van Belle, C. Claeys, E. Deckers, W. Desmet, On the impact of damping on the dispersion curves of a locally resonant metamaterial: Modelling and experimental validation, Journal of Sound and Vibration 409, doi:10.1016/j.jsv.2017.07.045.

[121] M. Oudich, Y. Li, B. M. Assouar, Z. Hou, A sonic band gap based on the locally resonant phononic plates with stubs, New Journal of Physics 12, doi:10.1088/1367-2630/12/8/083049.

[122] Y. Li, T. Chen, X. Wang, Y. Xi, Q. Liang, Enlargement of locally resonant sonic band gap by using composite plate-type acoustic metamaterial, Physics Letters, Section A: General, Atomic and Solid State Physics 379 (5), doi:10.1016/j.physleta.2014.11.028.

[123] M. I. Hussein, M. J. Leamy, M. Ruzzene, Dynamics of phononic materials and structures: Historical origins, recent progress, and future outlook, Applied Mechanics Reviews 66 (4), doi:10.1115/1.4026911.

[124] L. Brillouin, Wave Propagation in Periodic Structures (1946).

[125] C. Kittel, Introduction to Solid State Physics, 8th Edition, John Wiley & Sons, New York, 2004.

[126] N. G. R. de Melo Filho, C. Claeys, E. Deckers, W. Desmet, Metamaterial foam core sandwich panel designed to attenuate the mass-spring-mass resonance sound transmission loss dip, Mechanical Systems and Signal Processing 139, doi:10.1016/j.ymssp.2020.106624.

[127] B. R. Mace, D. Duhamel, M. J. Brennan, L. Hinke, Finite element prediction of wave motion in structural waveguides, The Journal of the Acoustical Society of America 117 (5), doi:10.1121/1.1887126.

[128] B. R. Mace, E. Manconi, Modelling wave propagation in two-dimensional structures using finite element analysis, Journal of Sound and Vibration 318 (4-5), doi:10.1016/j.jsv.2008.04.039.

[129] D. J. Mead, A General Theory of Harmonic Wave Propagation in Linear Periodic Systems with Multiple Coupling, Journal of Sound and Vibration 27 (2).

[130] D. Fritze, S. Marburg, H. J. Hardtke, Estimation of radiated sound power: A case study on common approximation methods, Acta Acustica united with Acustica 95 (5), doi:10.3813/AAA.918214.